

## Supporting Information

*Yumeng Li<sup>a</sup>, Yingmin Jin<sup>a,\*</sup>, Xin Zong<sup>a</sup>, Xuebai Zhang<sup>a</sup>, Guanshu Li<sup>b</sup>, Yueping Xiong<sup>a,\*</sup>*

<sup>a</sup> MIIT Key Laboratory of Critical Materials Technology for New Energy Conversion and Storage, School of Chemistry and chemical engineering, Harbin Institute of Technology, Harbin, 150001, P.R. China

<sup>b</sup> Key Laboratory of Science and Technology on Material Performance Evaluating in Space Environment, School of Materials Science and Engineering, Harbin Institute of Technology, Harbin, 150001, P.R. China

\*E-mail address: [jymjinyingmin@163.com](mailto:jymjinyingmin@163.com) (Y. Jin) [ypxiong@hit.edu.cn](mailto:ypxiong@hit.edu.cn) (Y. Xiong)

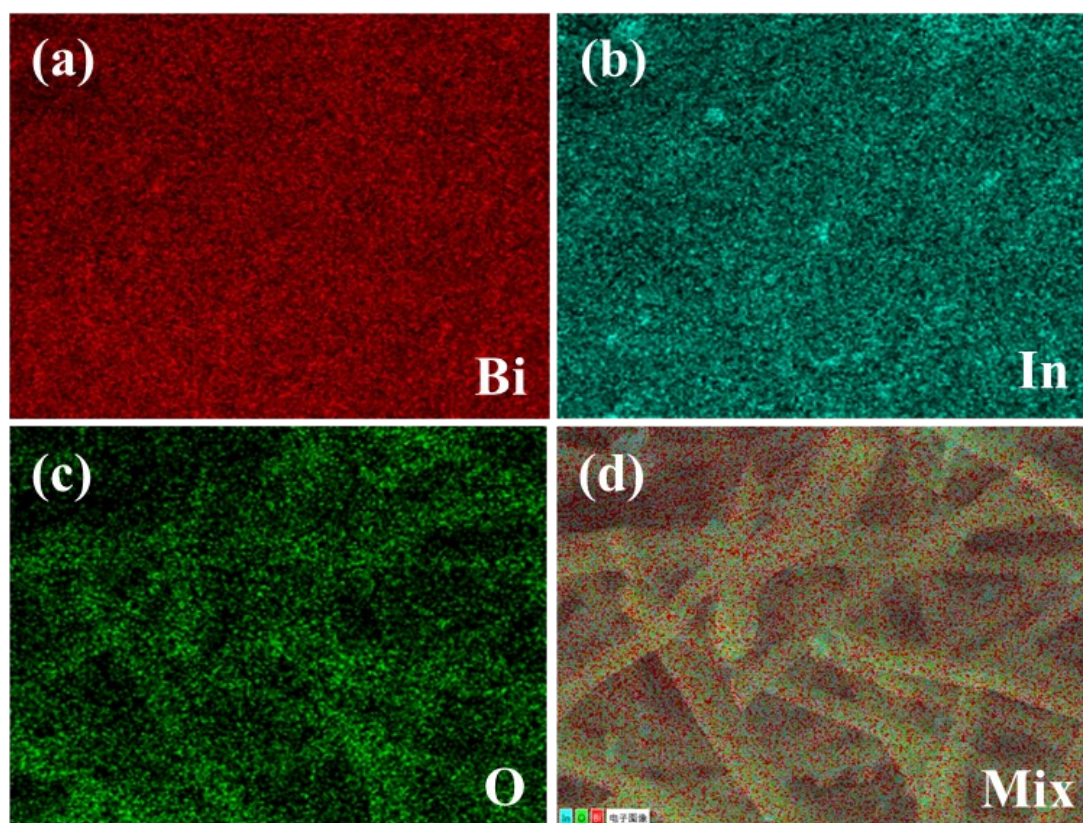


**Fig. S1.** the corresponding EDS mappings of (a) Bi, (b) In, (C) O, and (d) Mix for  $\text{Bi}_5\text{In}_5$  oxide precursor NFs.

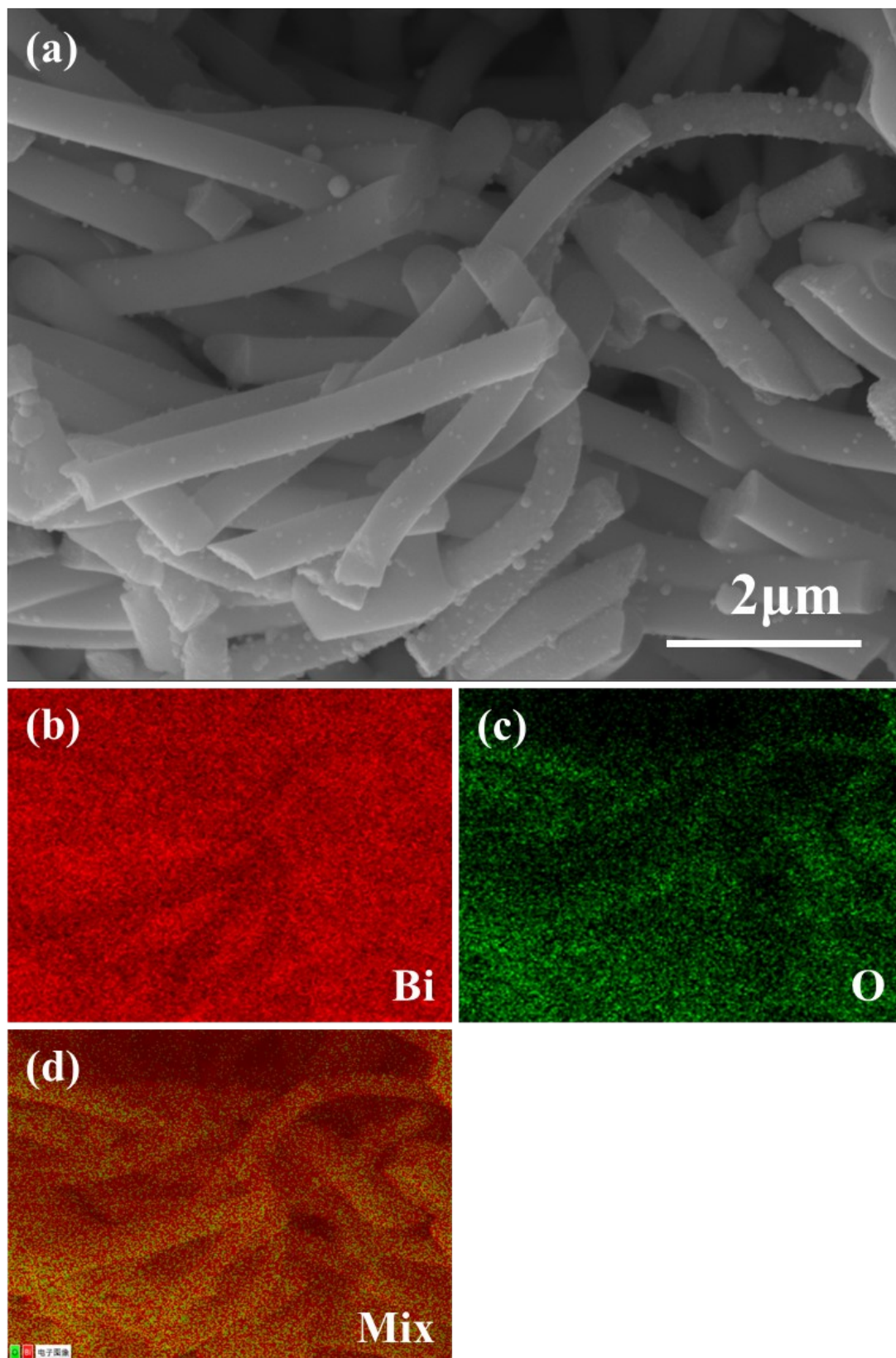


**Fig. S2.** (a) SEM image and (b, c, and d) the corresponding EDS mappings of the Bi oxide precursor NFs.

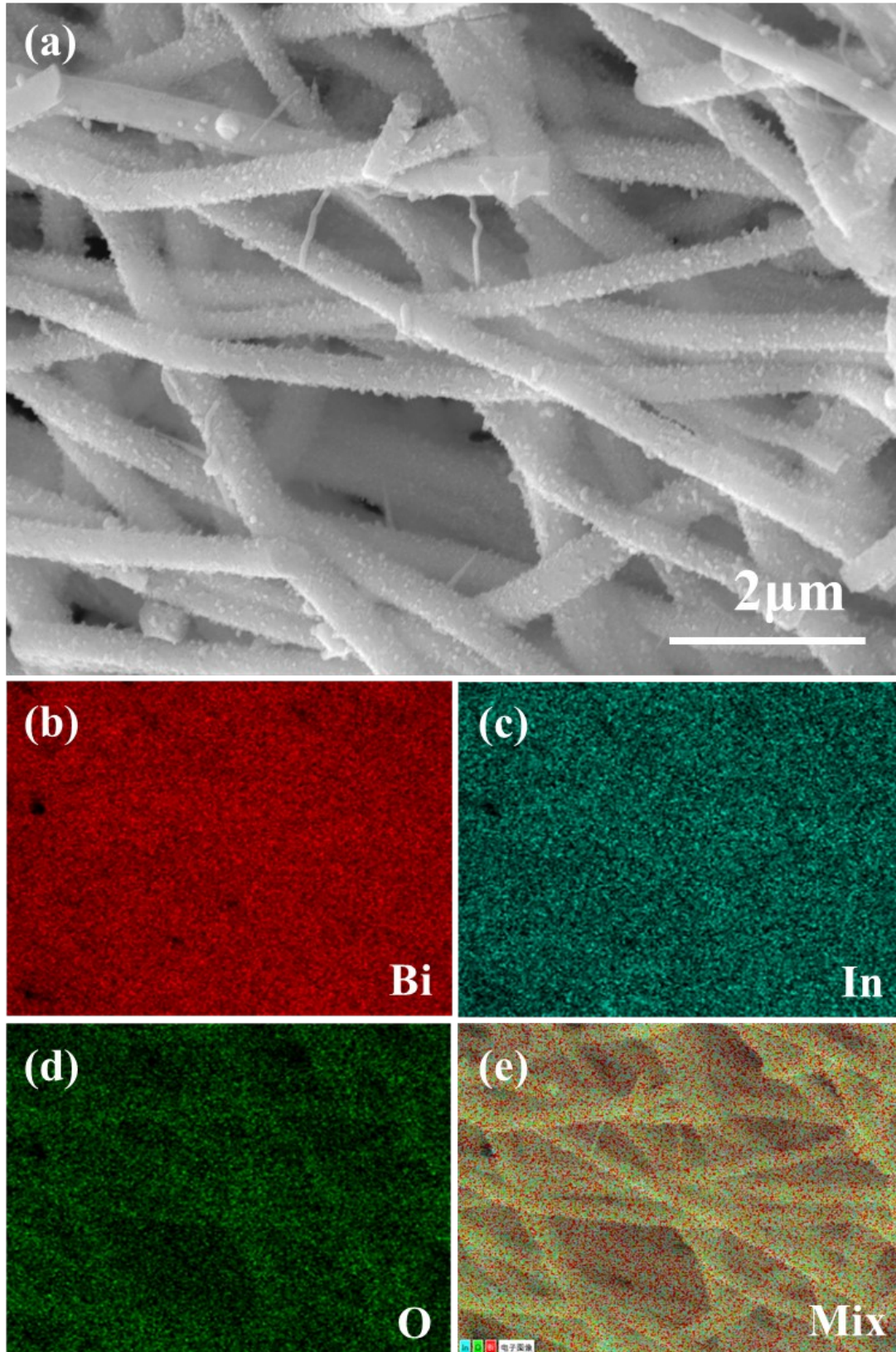


**Fig. S3.** (a) SEM image and (b, c, d and e) the corresponding EDS mappings of the  $\text{Bi}_7\text{In}_3$  oxide precursor NFs.

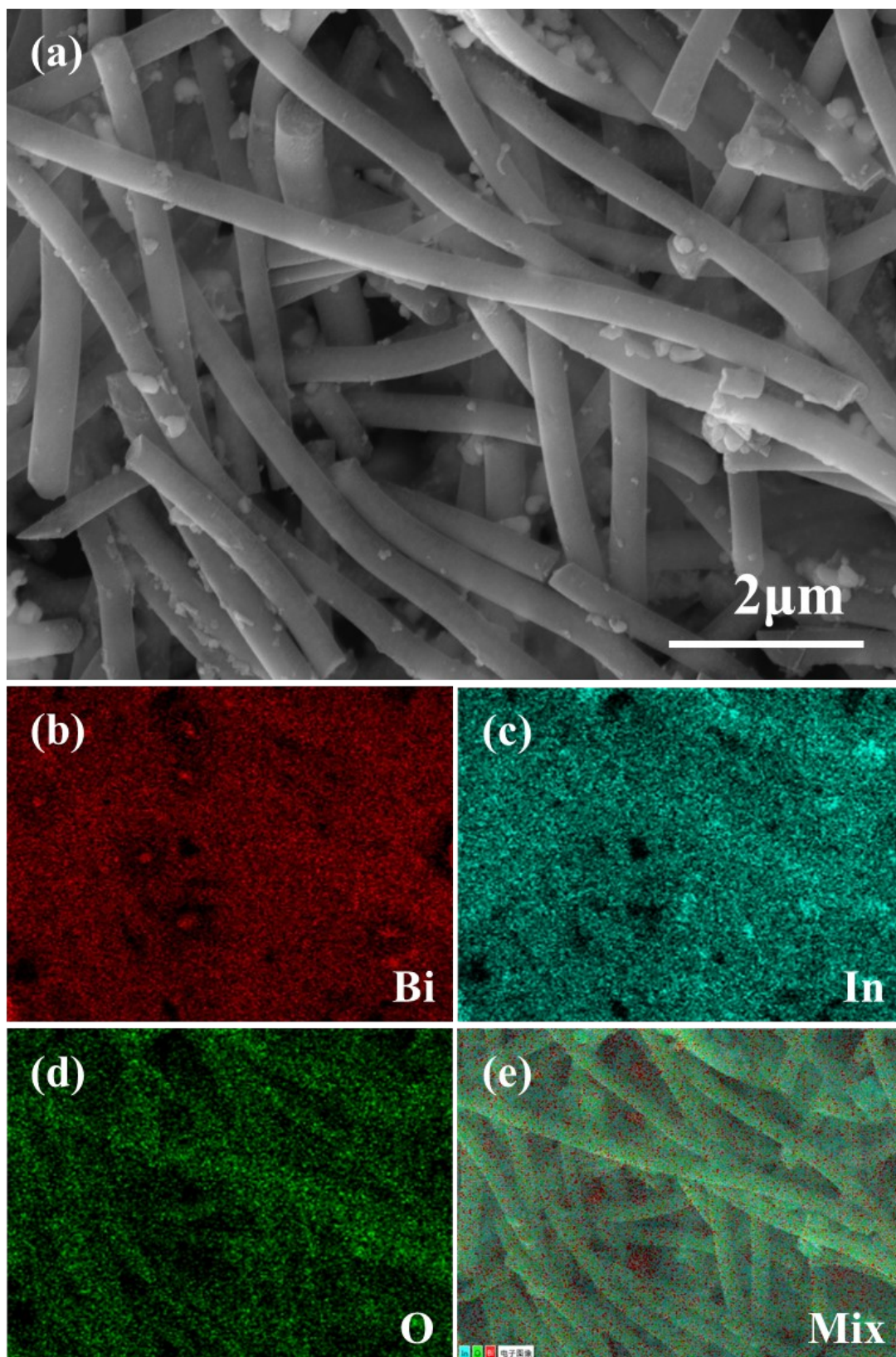


**Fig. S4.** (a) SEM image and (b, c, d and e) the corresponding EDS mappings of the  $\text{Bi}_3\text{In}_7$  oxide precursor NFs.

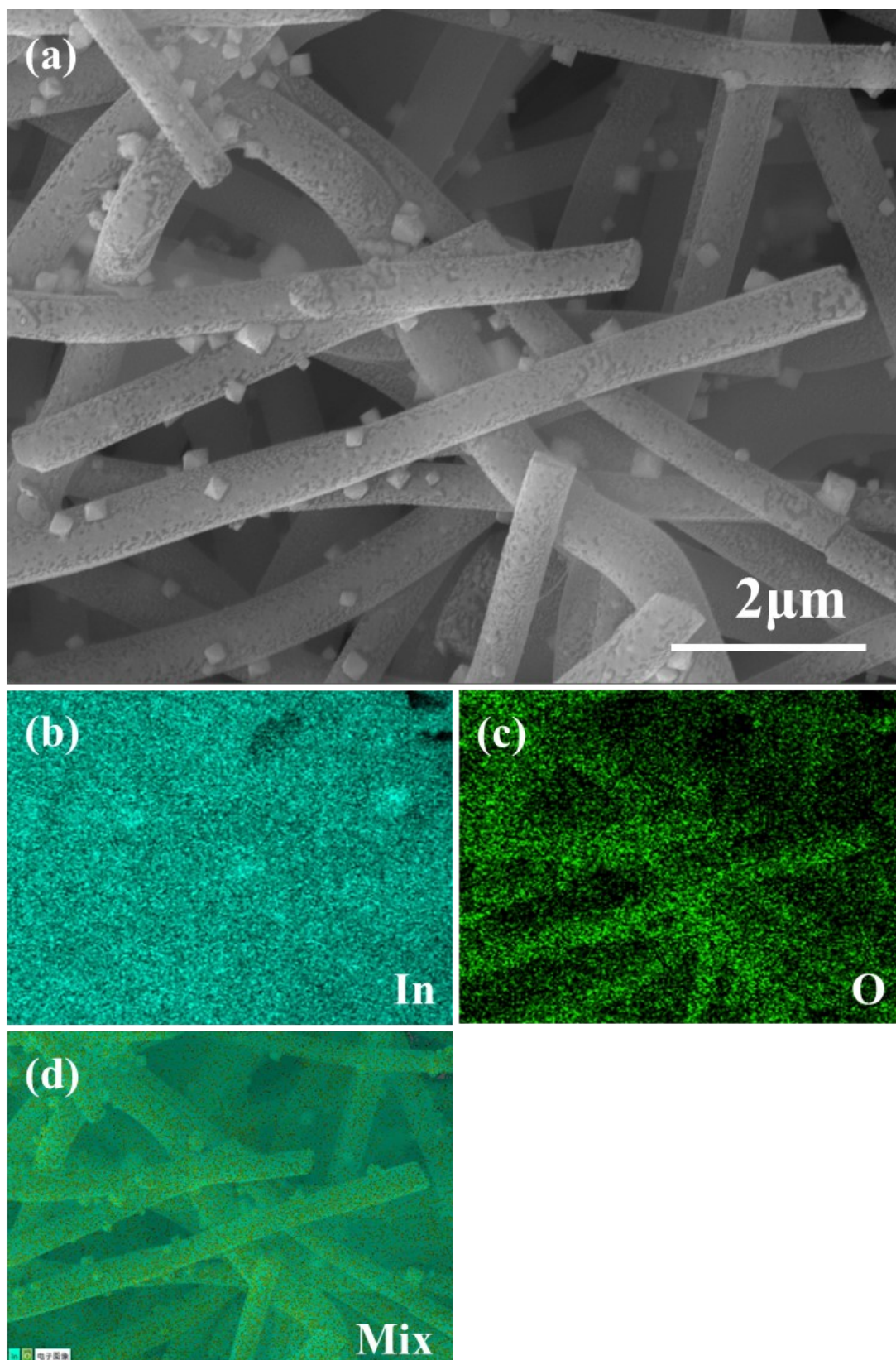


**Fig. S5.** (a) SEM image and (b, c, and d) the corresponding EDS mappings of the In oxide precursor NFs.

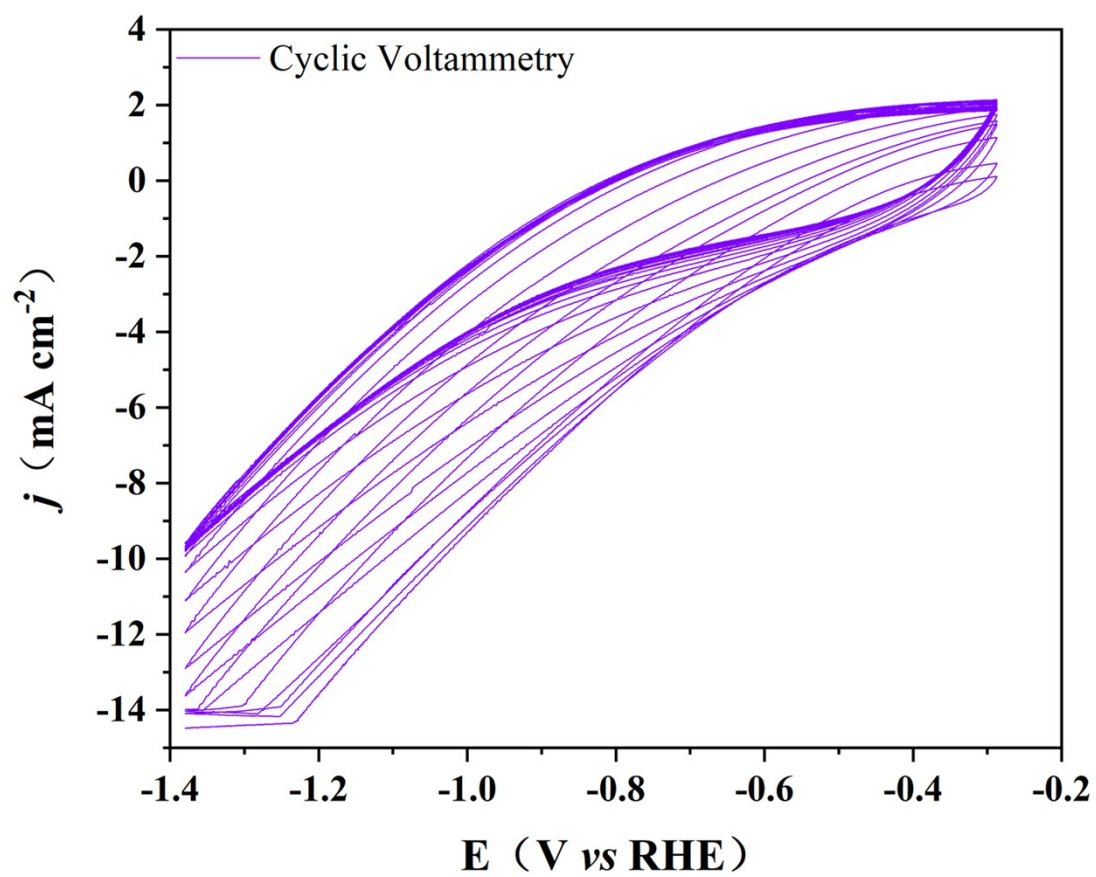
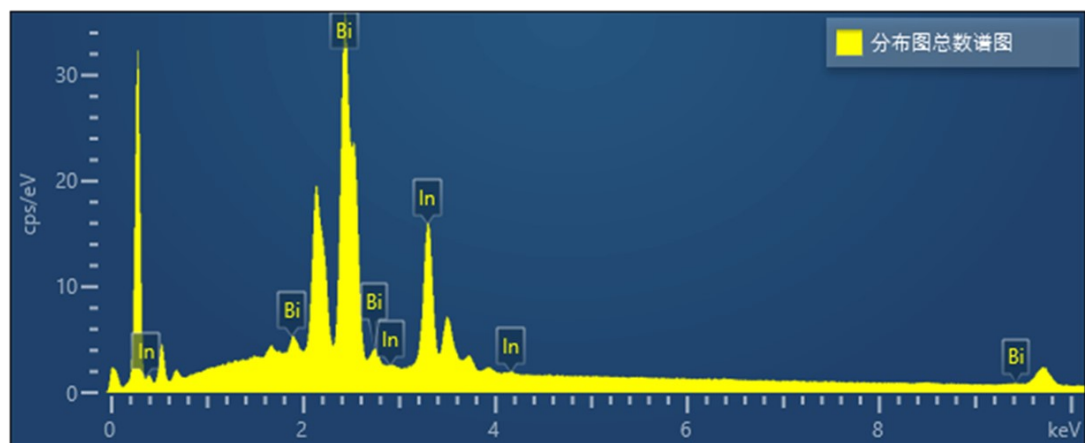
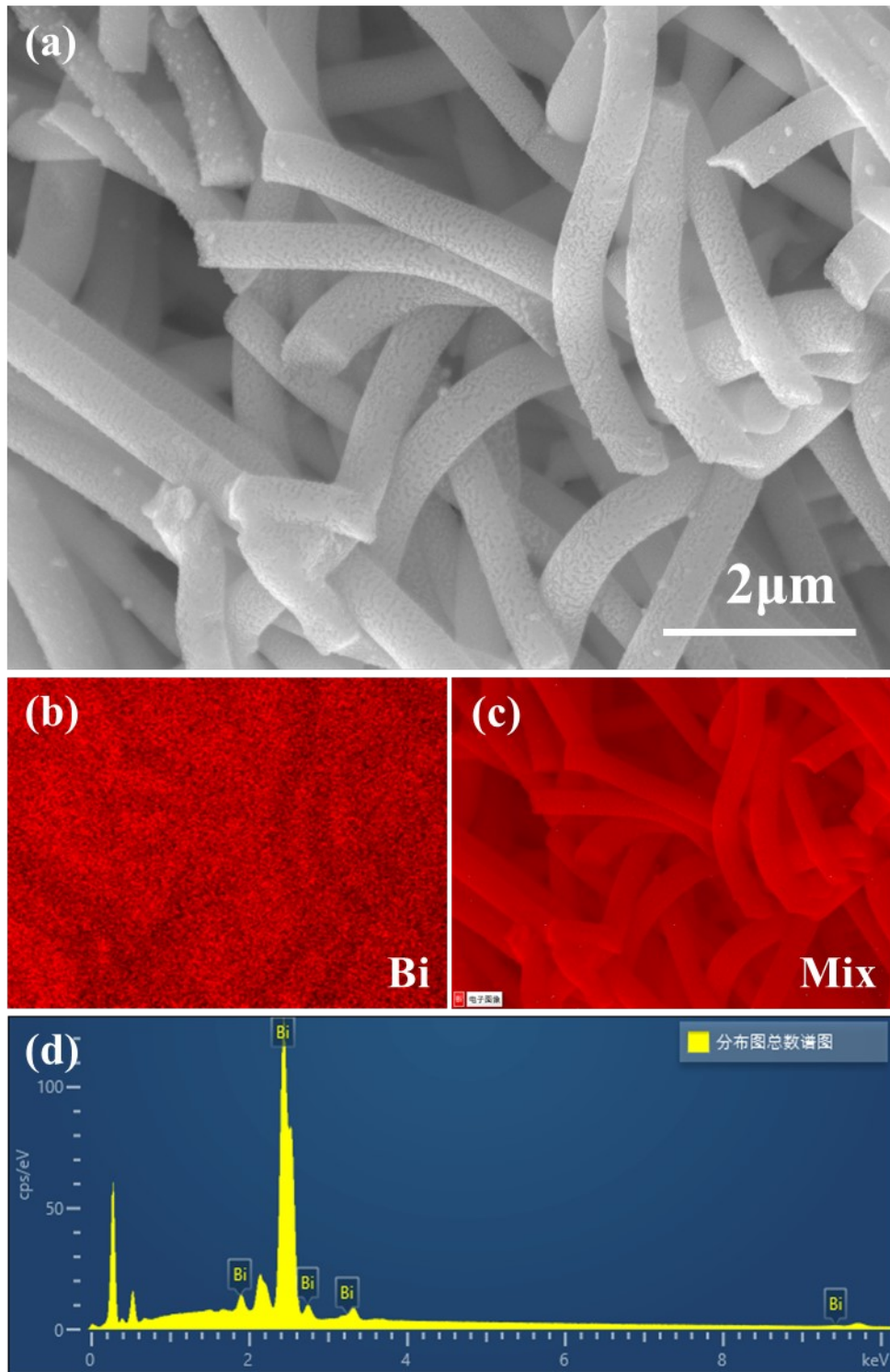


Fig. S6. the electrochemical reducing current-voltage curve.



**Fig. S7.** EDS of Bi<sub>5</sub>In<sub>5</sub> NFs.



**Fig. S8.** (a) SEM image and (b, c, and d) the corresponding EDS and mappings of the Bi NFs.



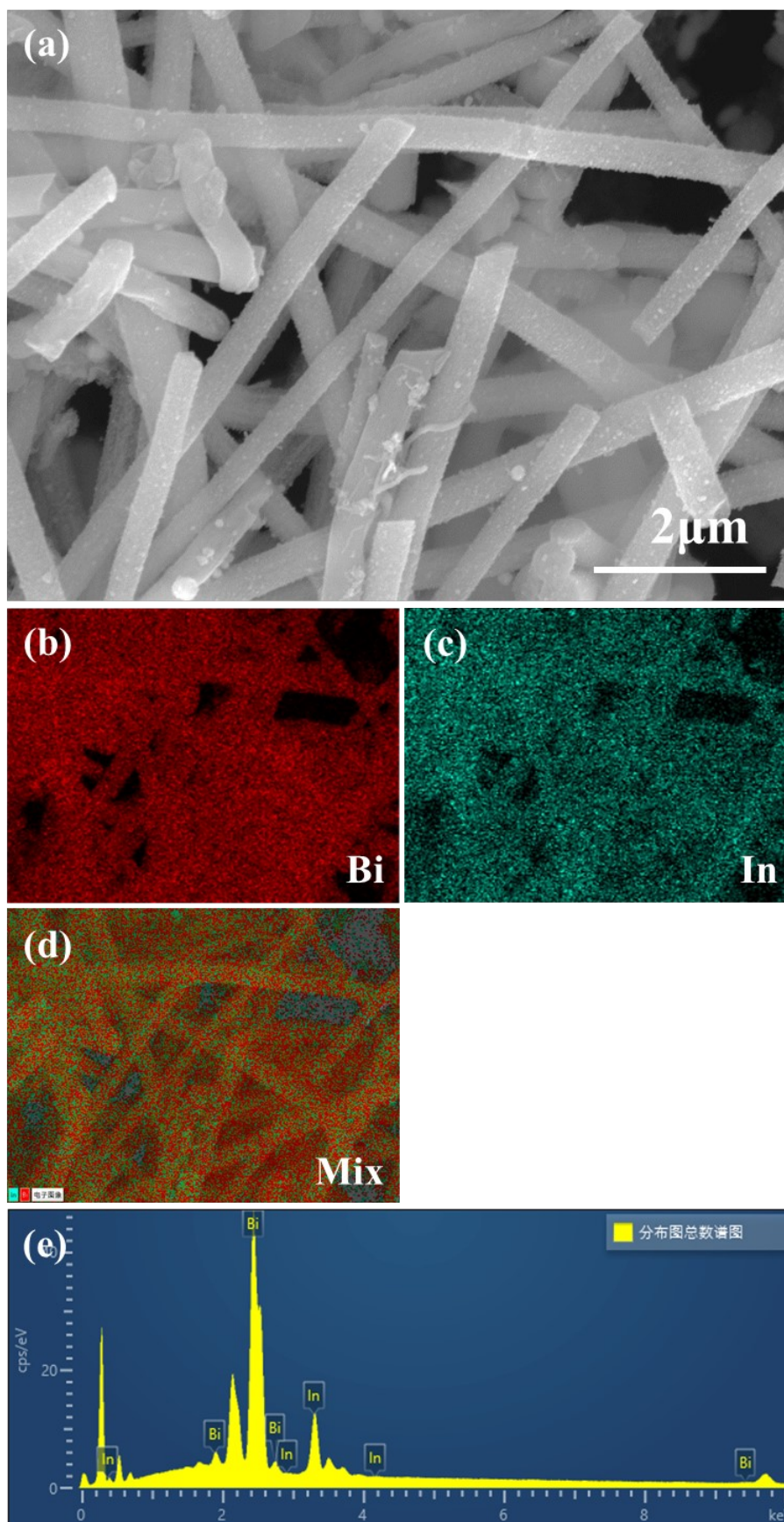


**Fig. S9.** (a) SEM image and (b, c, d and e) the corresponding EDS and mappings of the  $\text{Bi}_7\text{In}_3$  NFs.

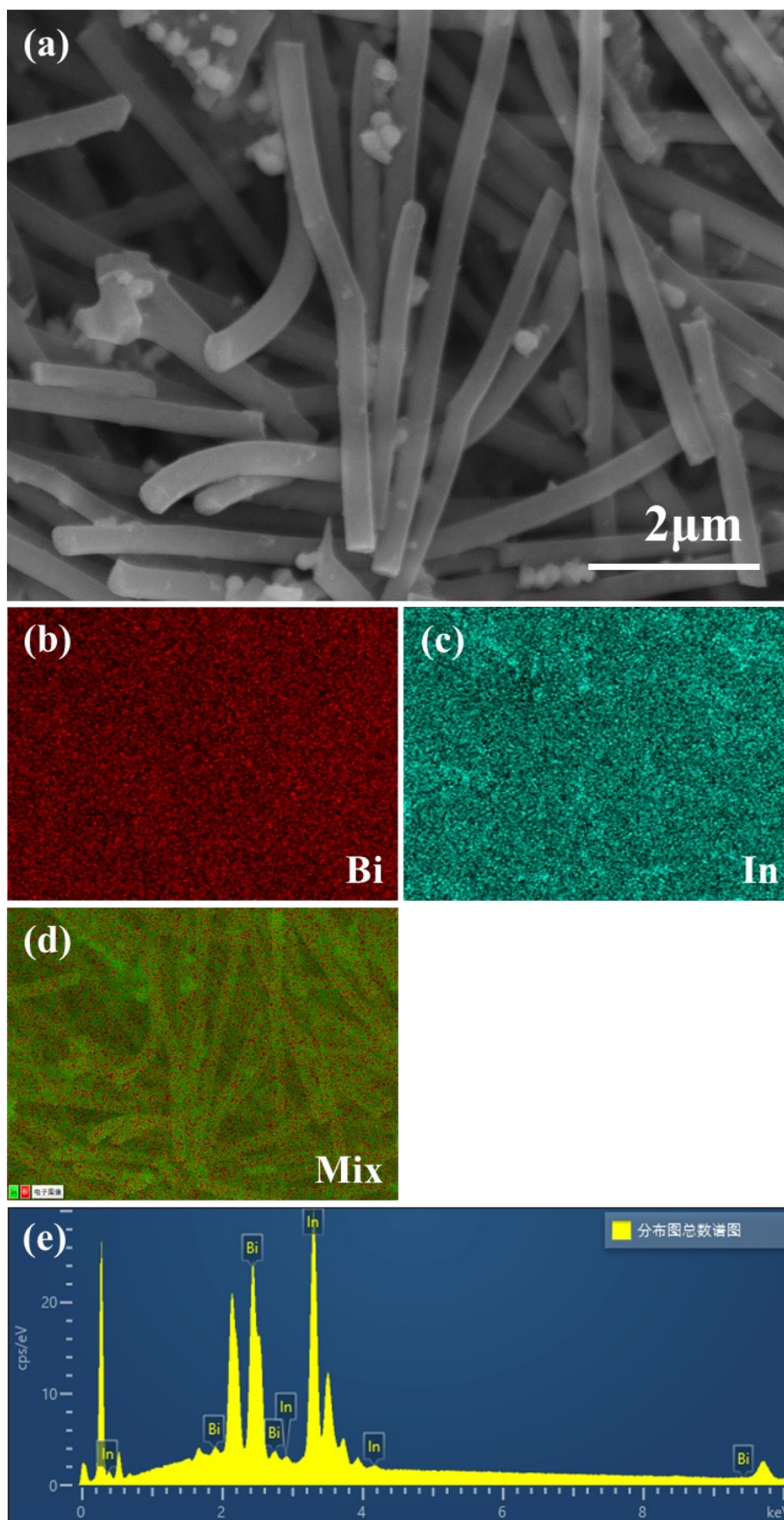


**Fig. S10.** (a) SEM image and (b, c, d and e) the corresponding EDS and mappings of the  $\text{Bi}_3\text{In}_7$  NFs.

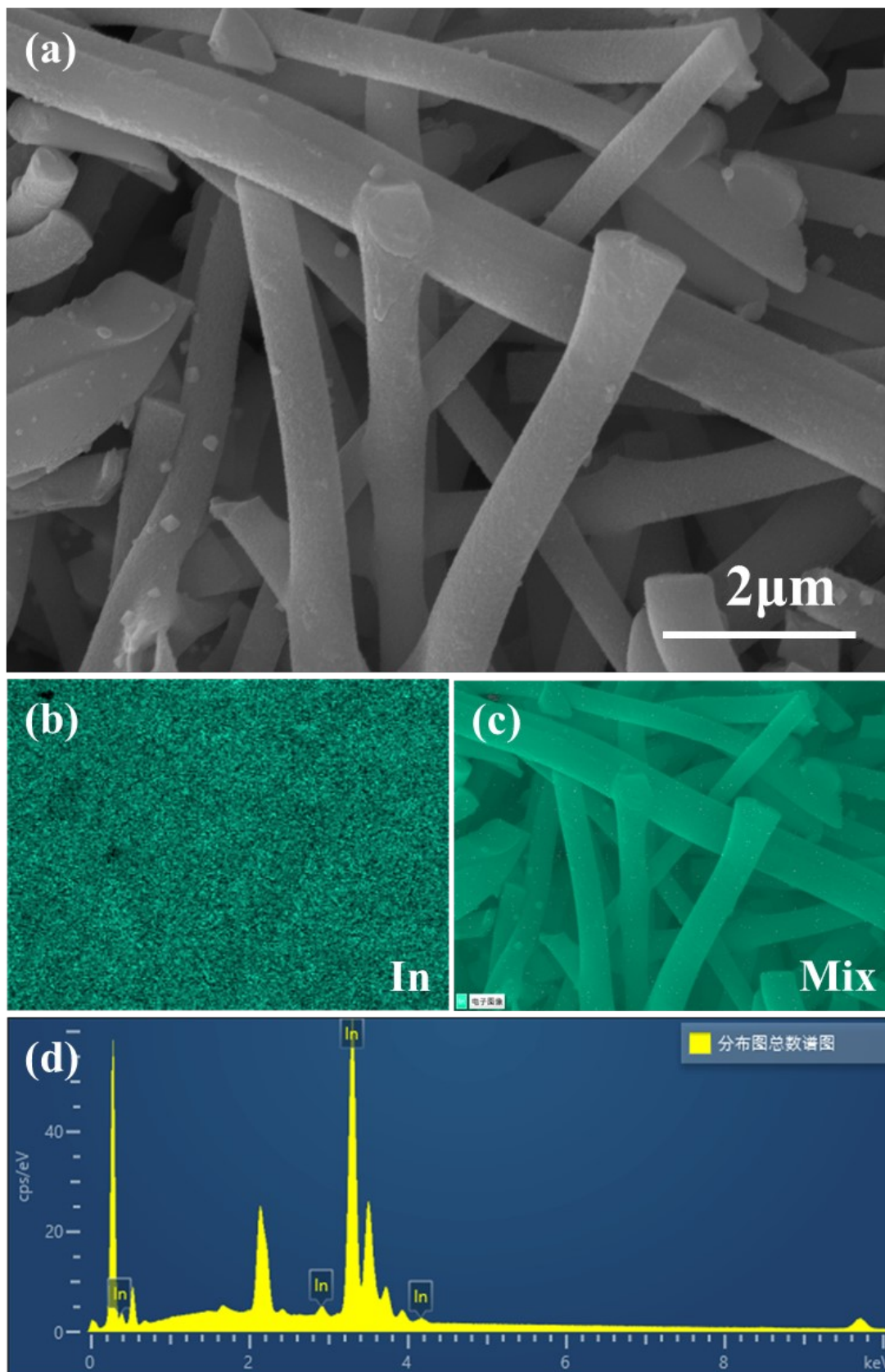


**Fig. S11.** (a) SEM image and (b, c, d and e) the corresponding EDS and mappings of the Bi<sub>3</sub>In<sub>7</sub> NFs.

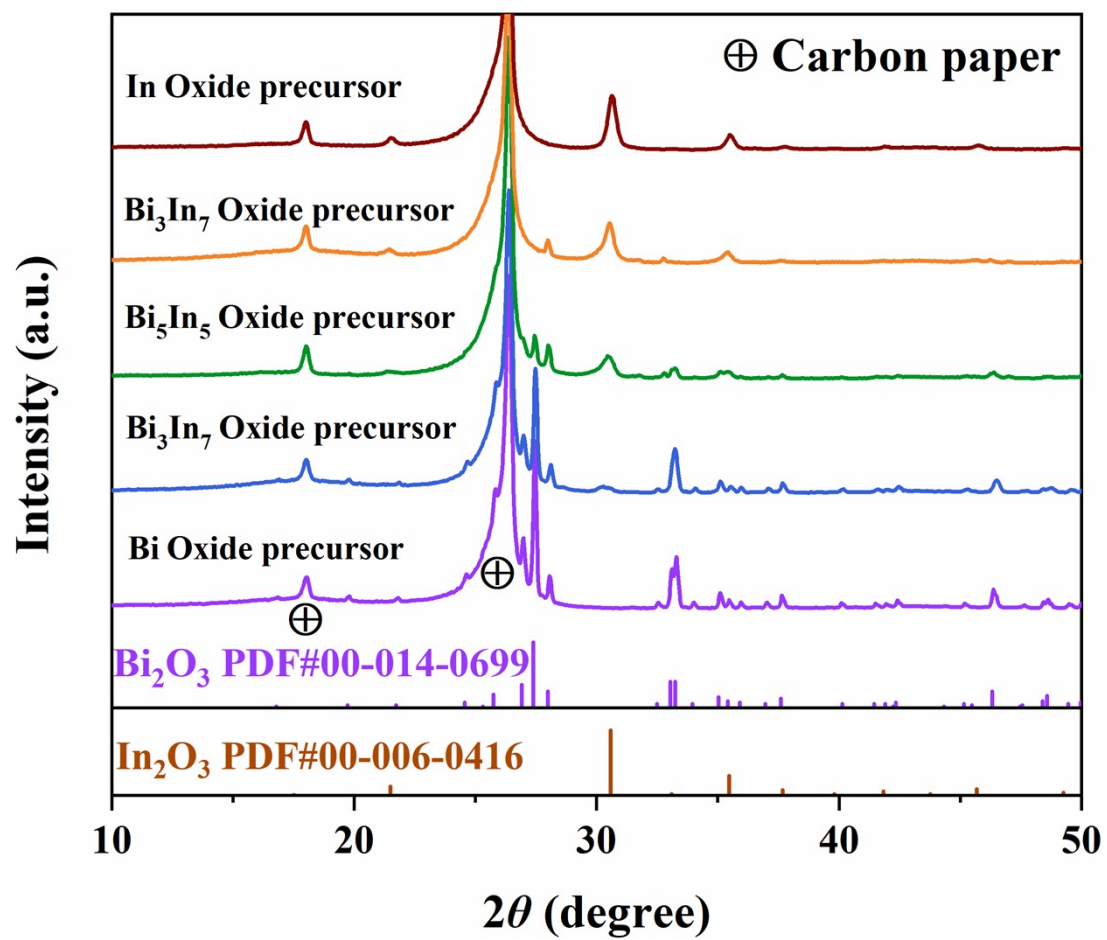
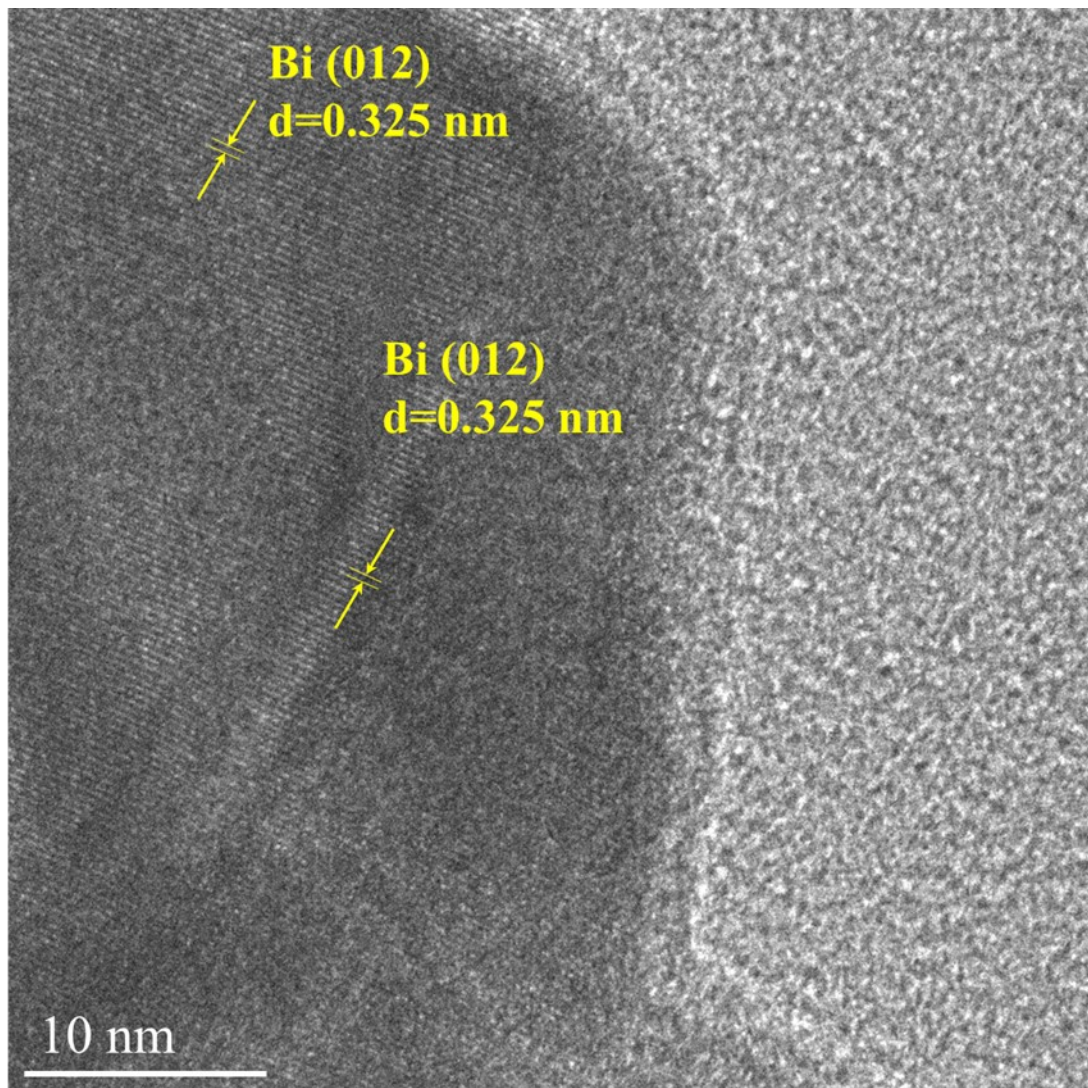
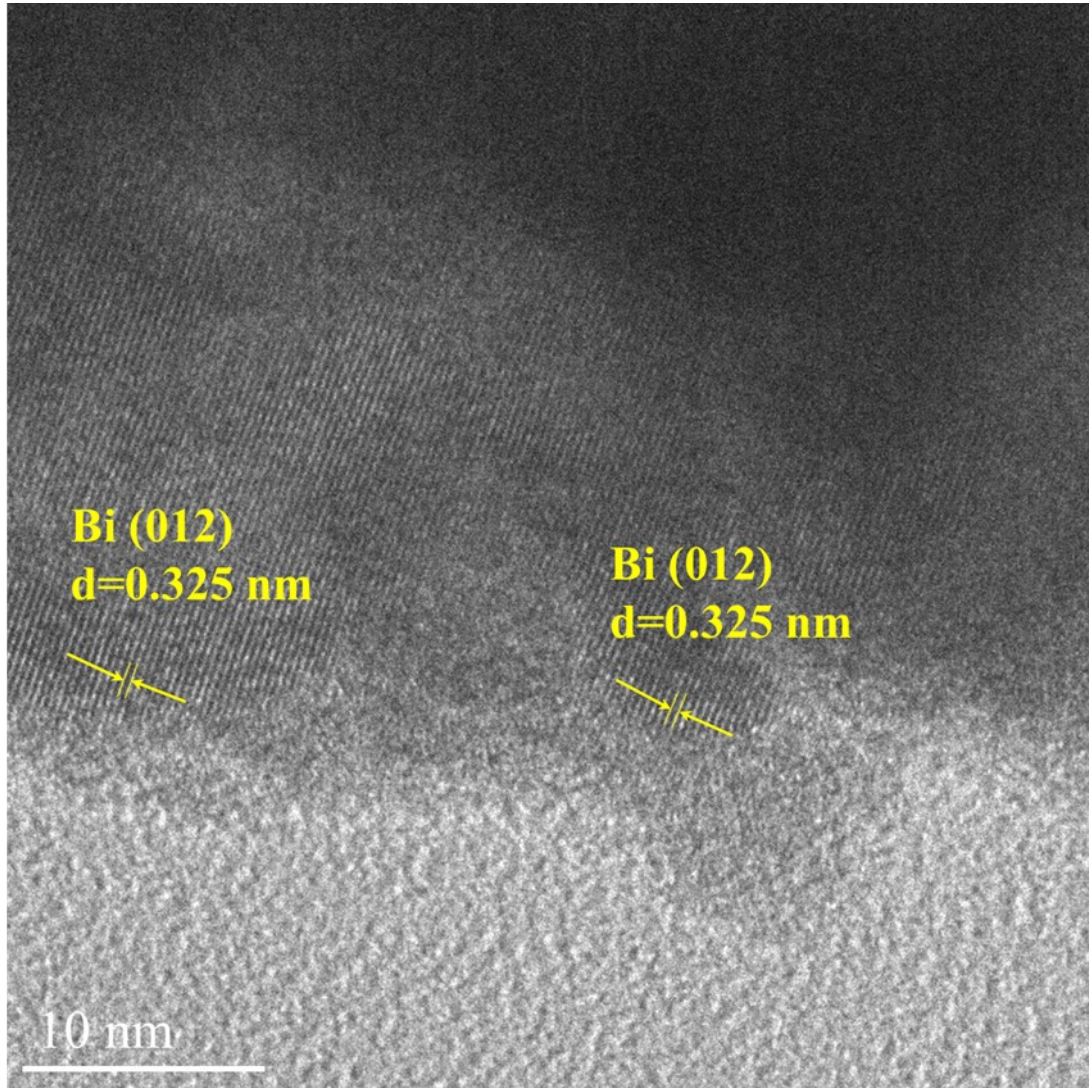


Fig. S12. XRD patterns of the oxide precursor NFs.



**Fig. S13.** HRTEM of Bi.



**Fig. S14.** HRTEM of  $\text{Bi}_7\text{In}_3$ .

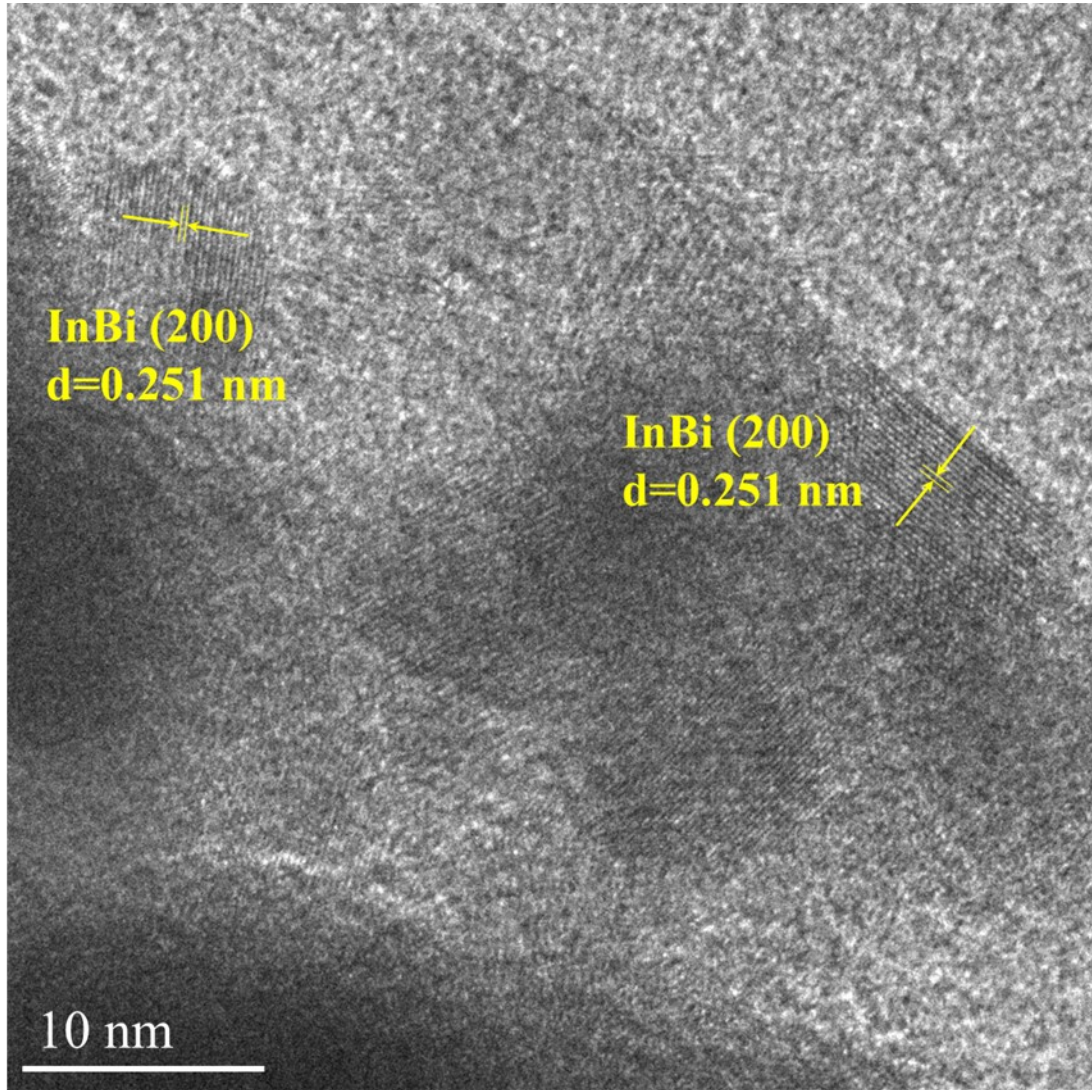


**Fig. S15.** HRTEM of  $\text{Bi}_5\text{In}_5$ .

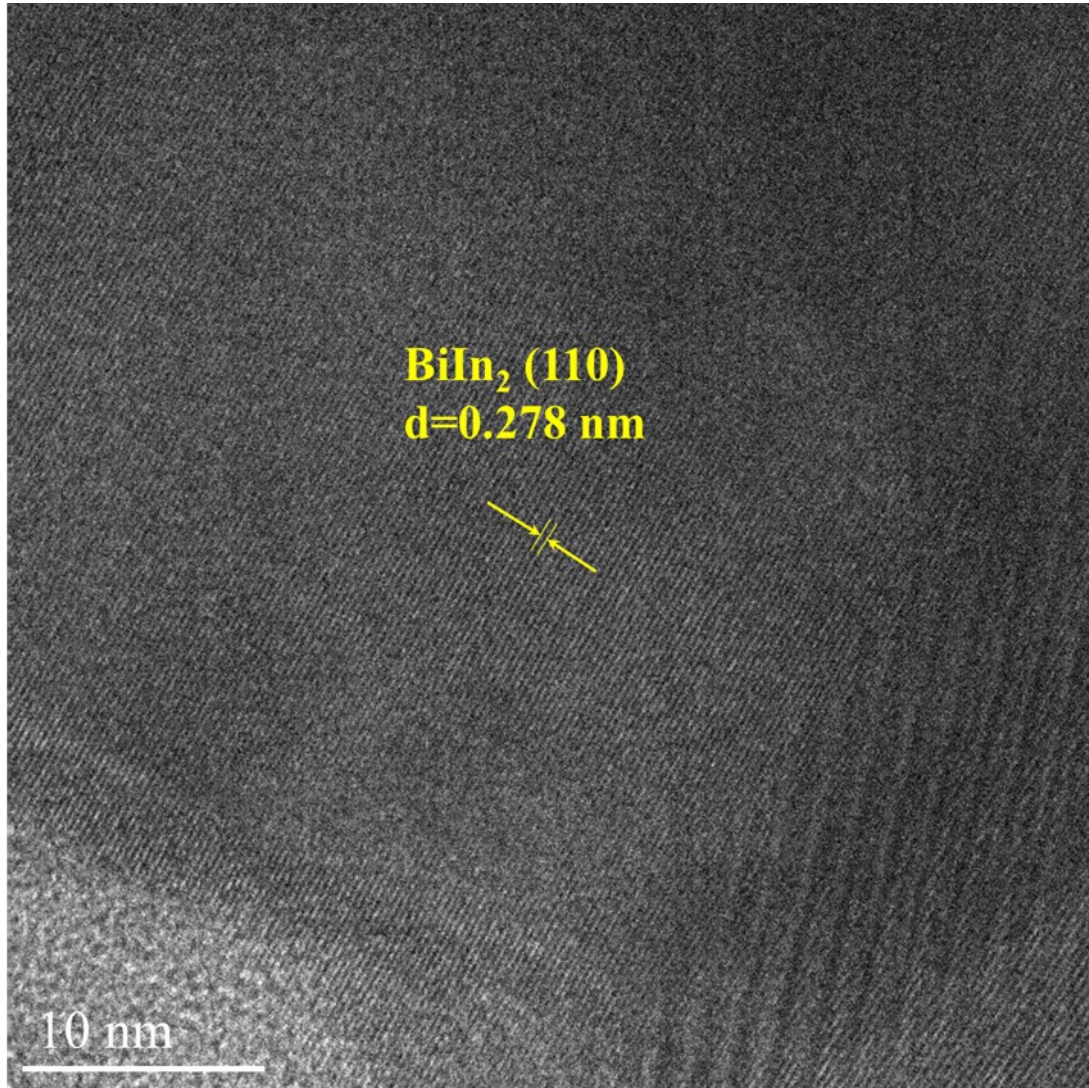


**Fig. S16.** HRTEM of Bi<sub>3</sub>In<sub>7</sub>.



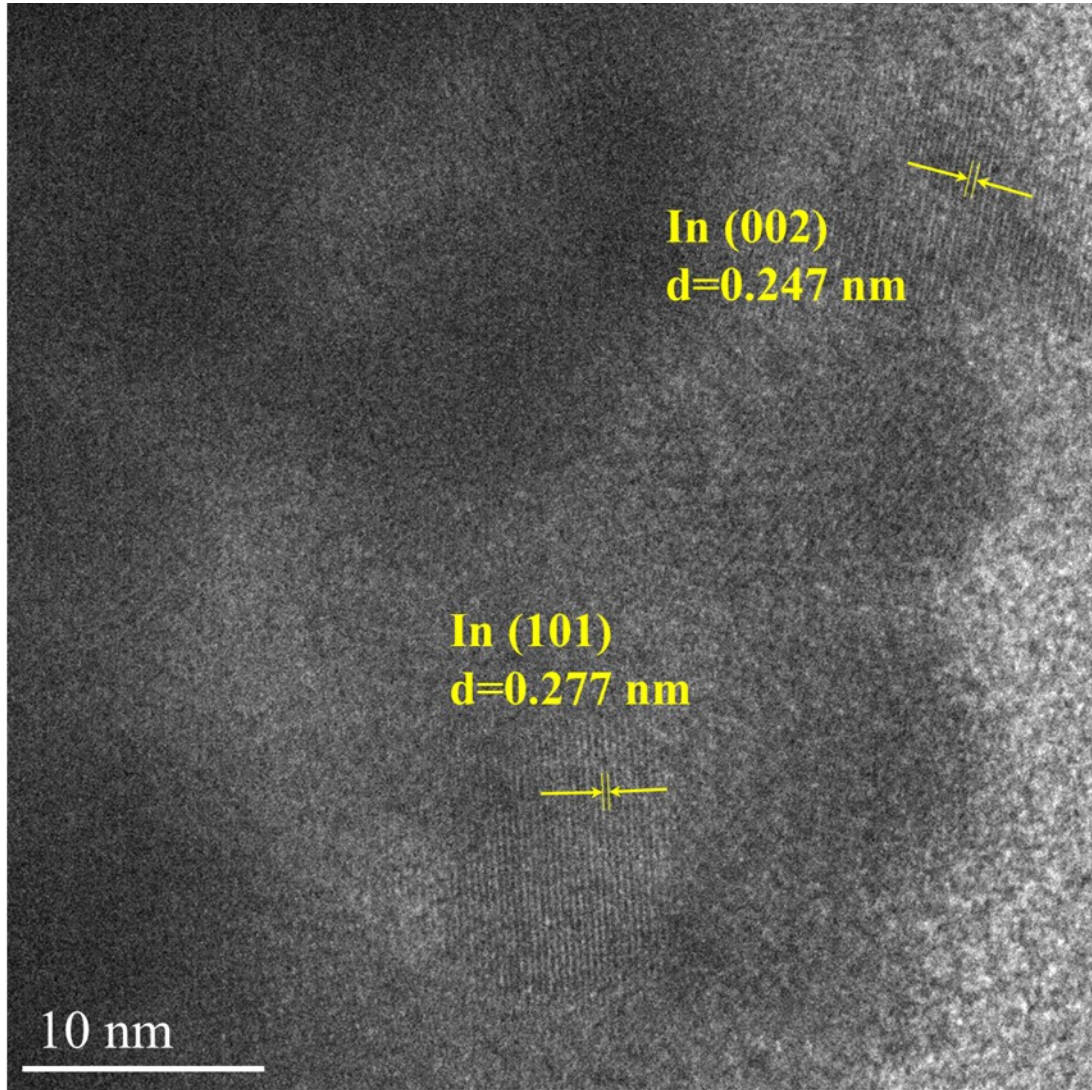


**Fig. S17.** HRTEM of In.

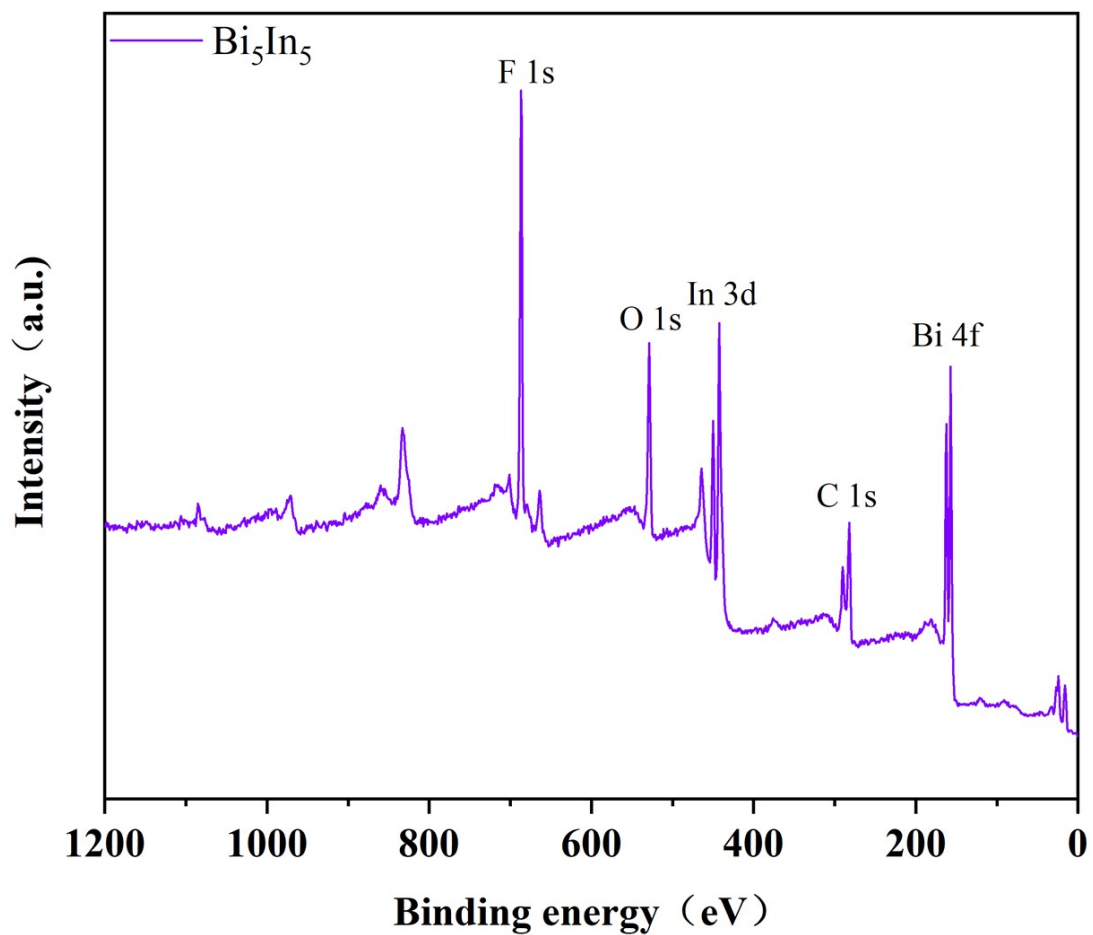


**Fig. S18.** full range XPS spectrum of the  $\text{Bi}_5\text{In}_5$  NFs.

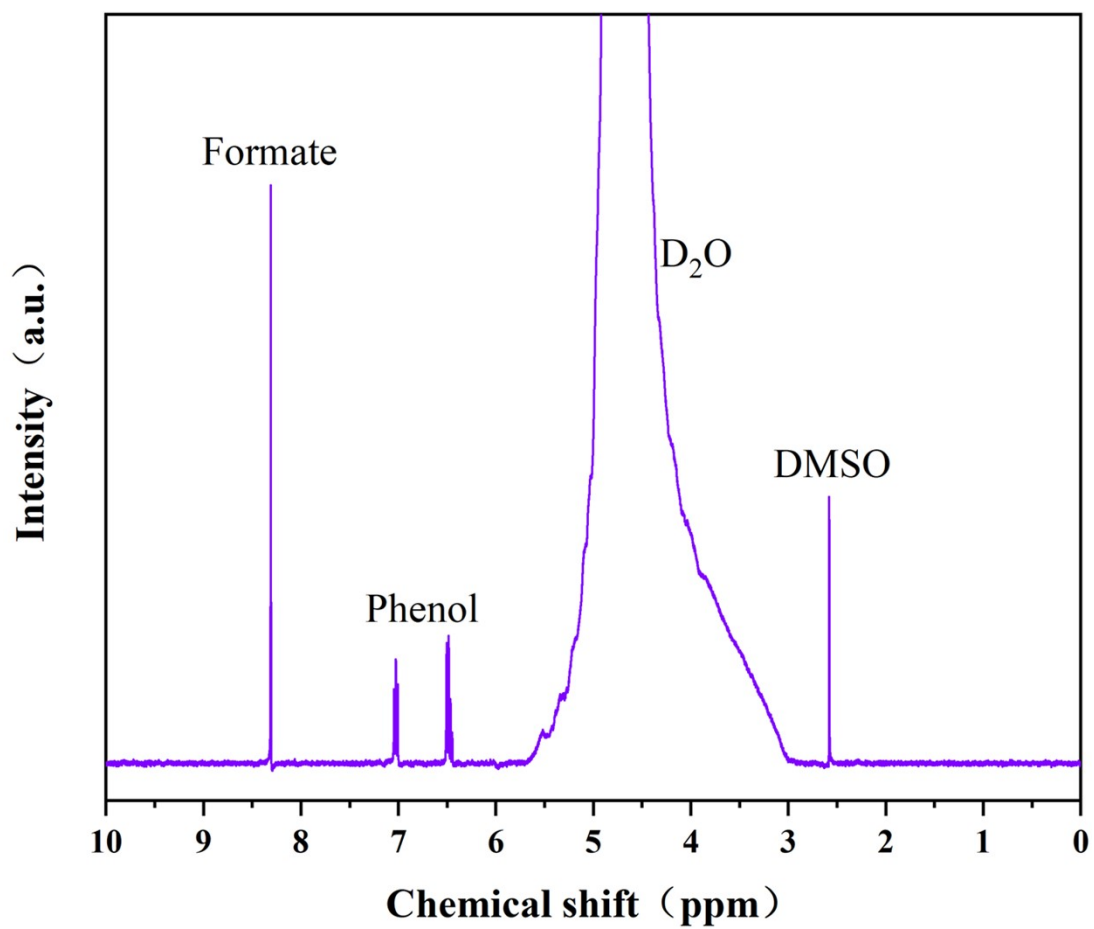


**Fig. S19.**  $^1\text{H}$  NMR spectra of the  $\text{Bi}_5\text{In}_5$  NFs.

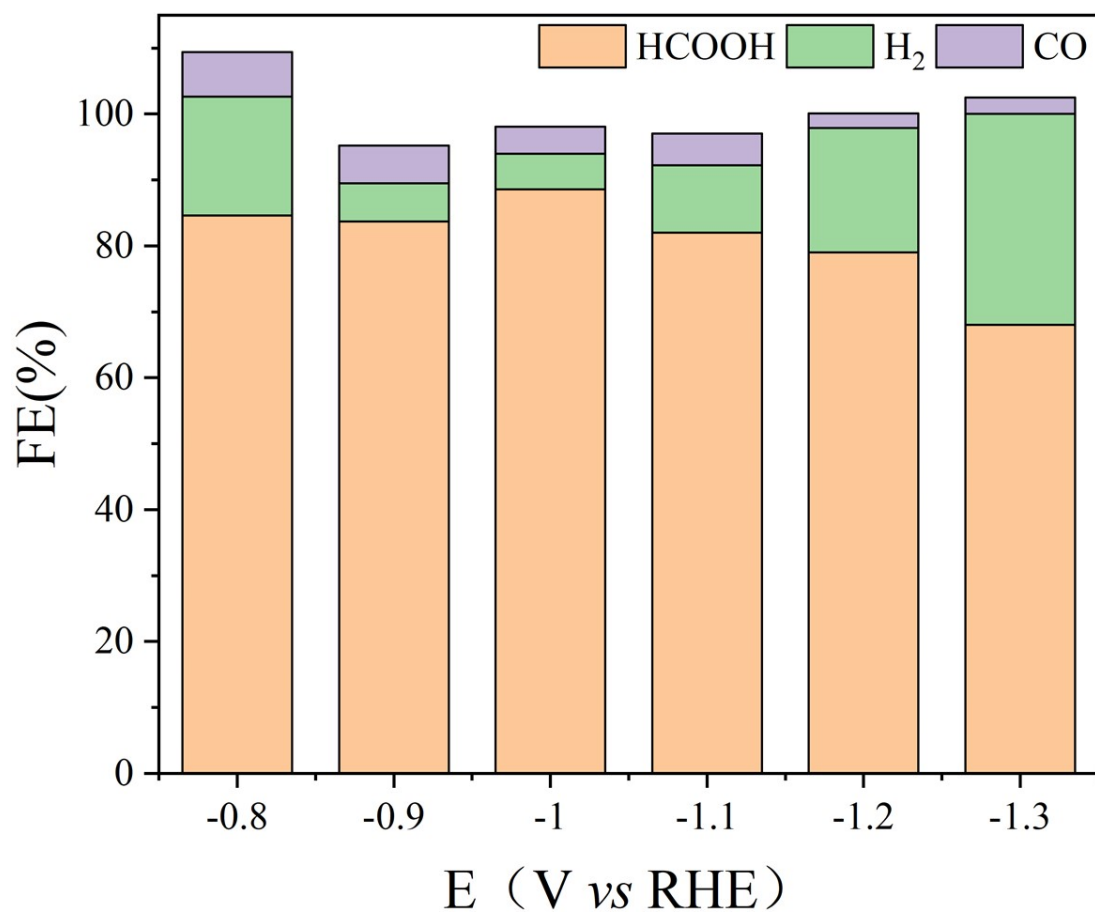


**Fig. S20.** FE for HCOOH, H<sub>2</sub>, CO at different potentials on Bi NF.

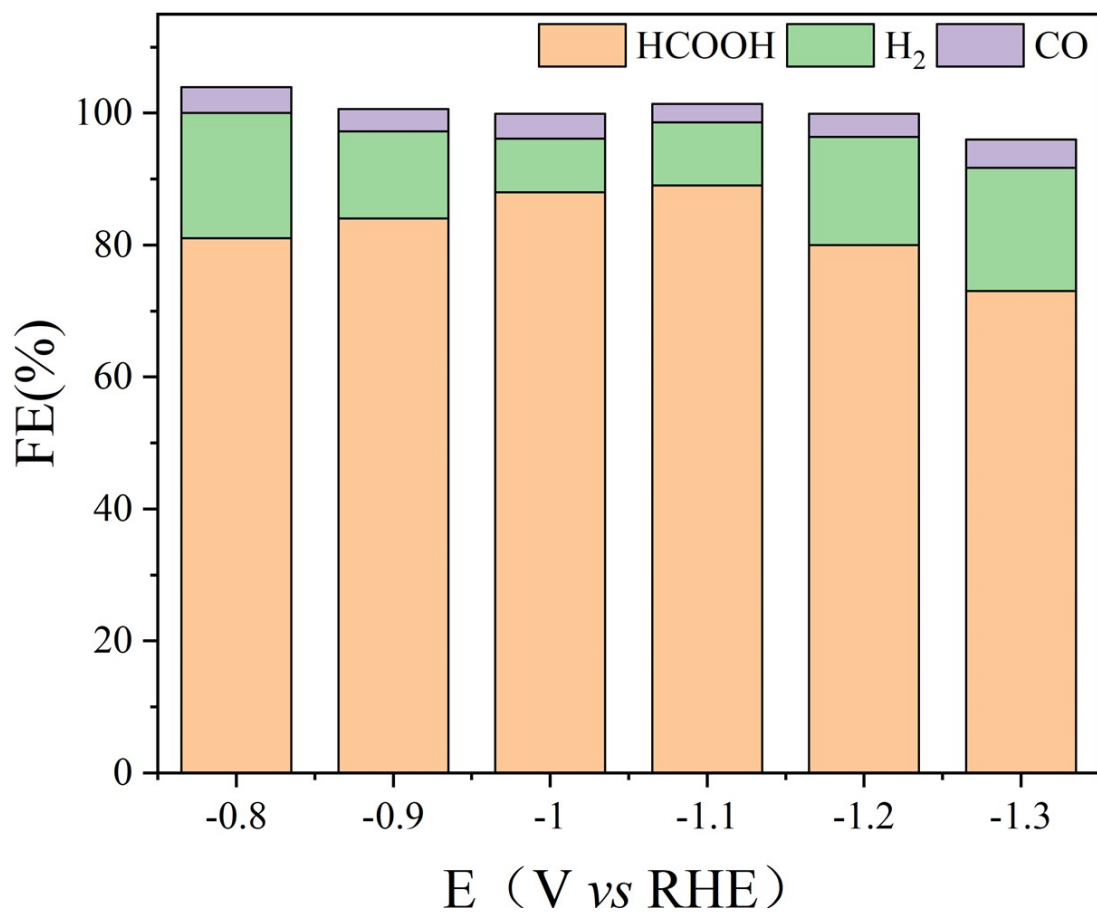


**Fig. S21.** FE for HCOOH, H<sub>2</sub>, CO at different potentials on Bi<sub>7</sub>In<sub>3</sub> NF.

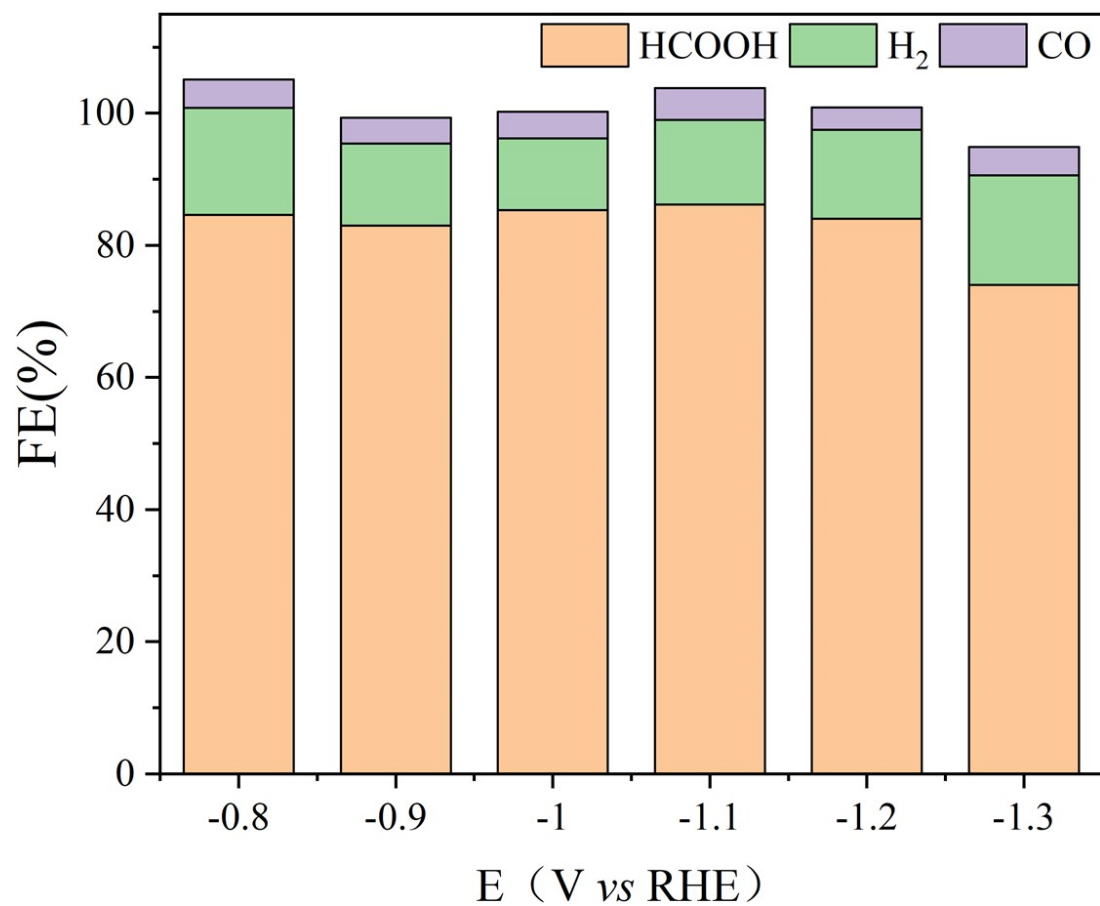


**Fig. S22.** FE for HCOOH, H<sub>2</sub>, CO at different potentials on Bi<sub>3</sub>In<sub>7</sub> NF.

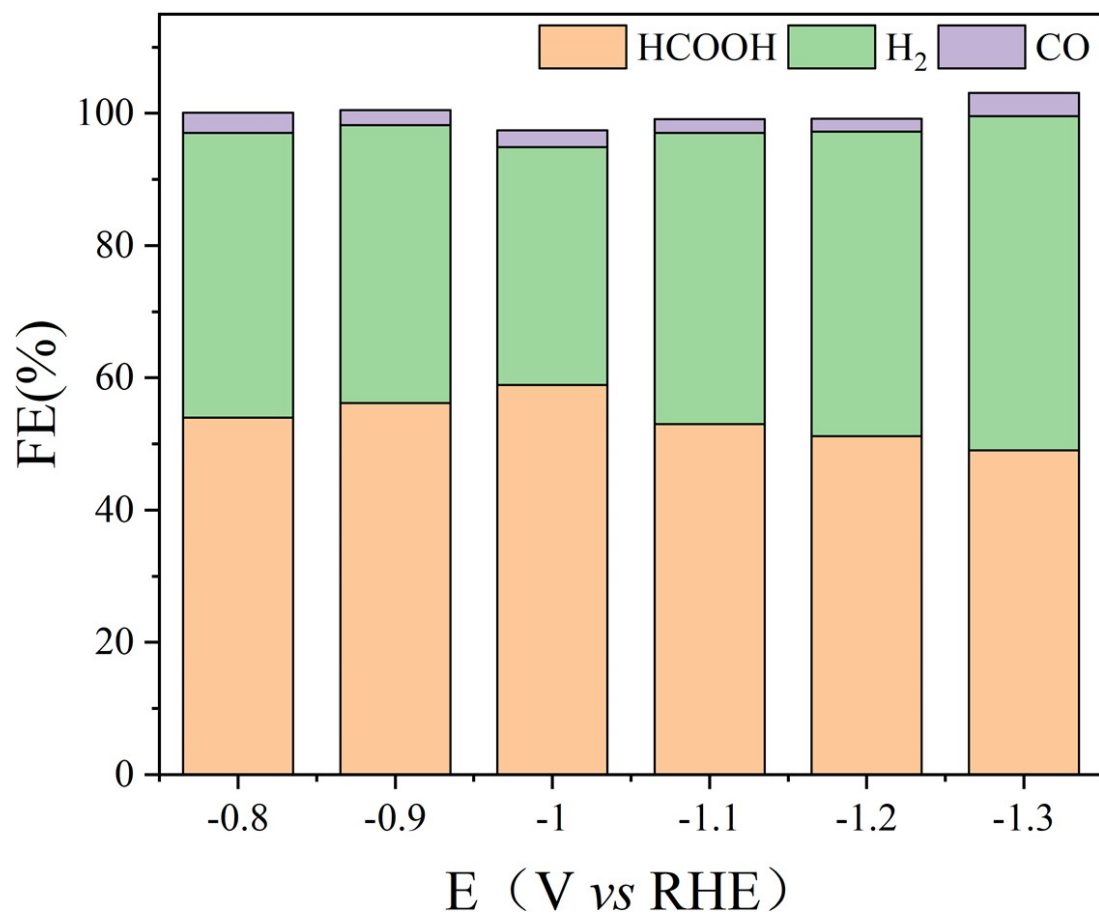


**Fig. S23.** FE for HCOOH, H<sub>2</sub>, CO at different potentials on In NF.

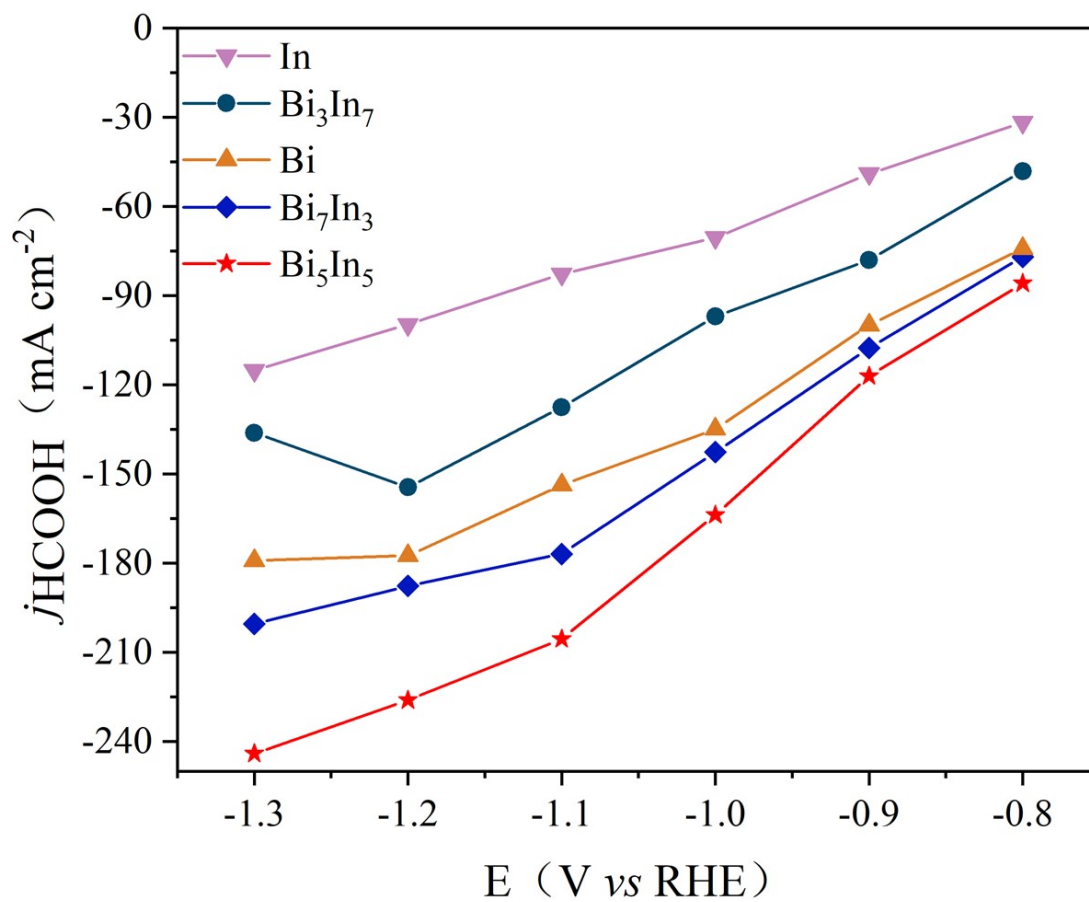


**Fig. S24.** Partial current densities of HCOOH on Bi<sub>x</sub>In<sub>y</sub> NFs.



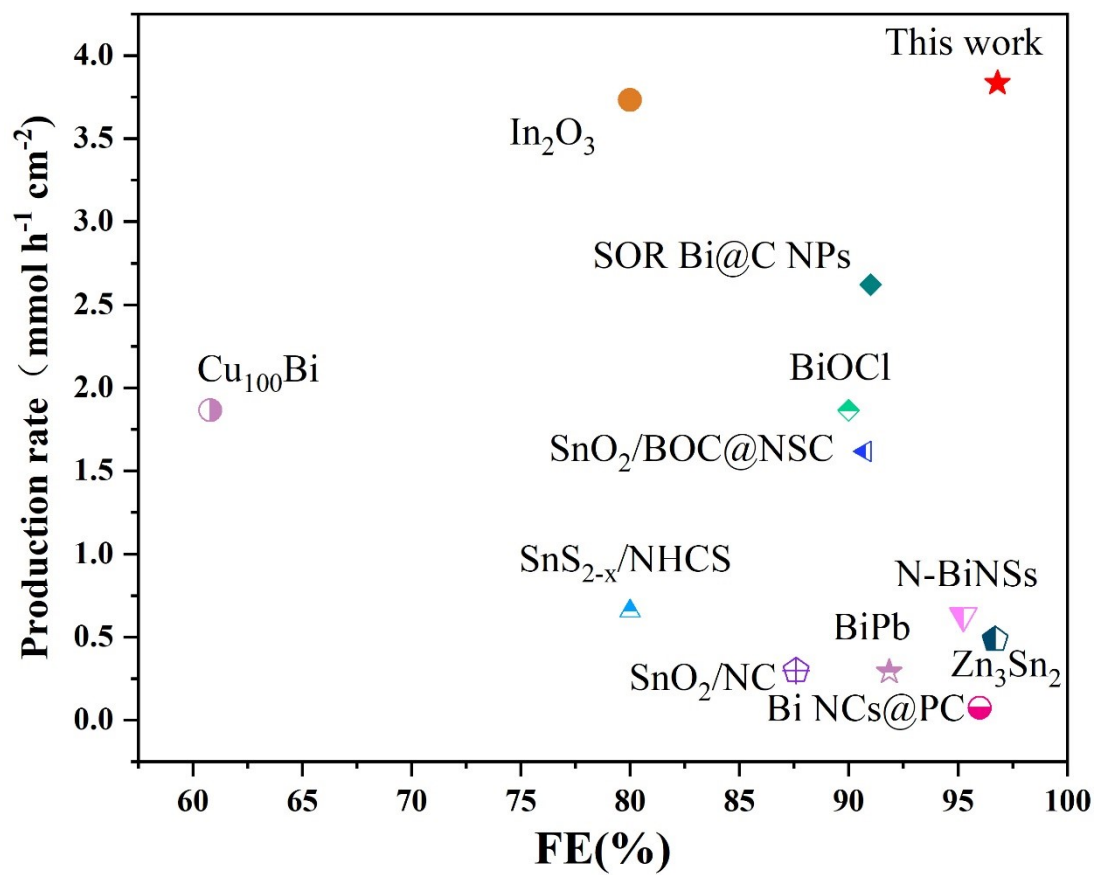
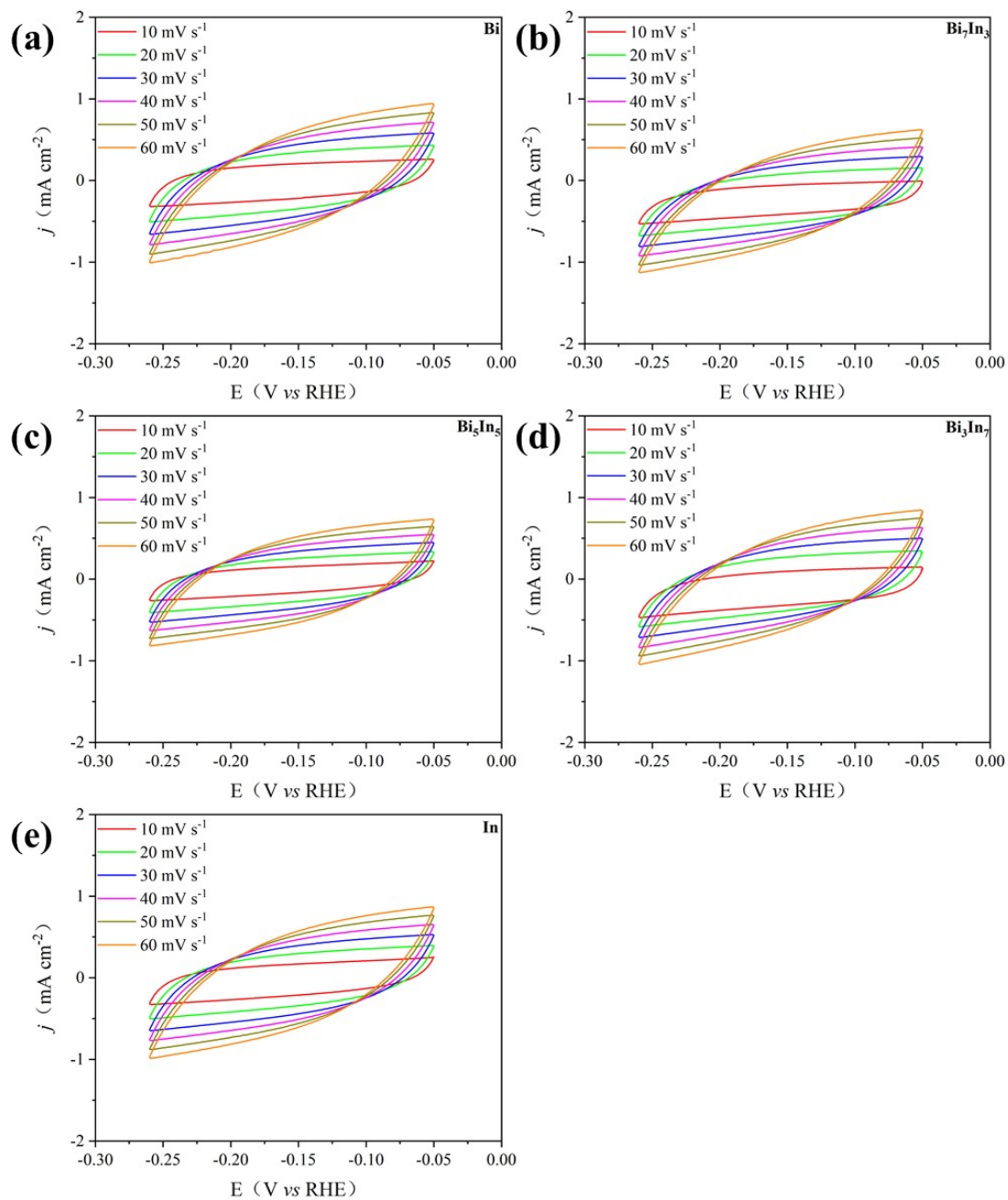
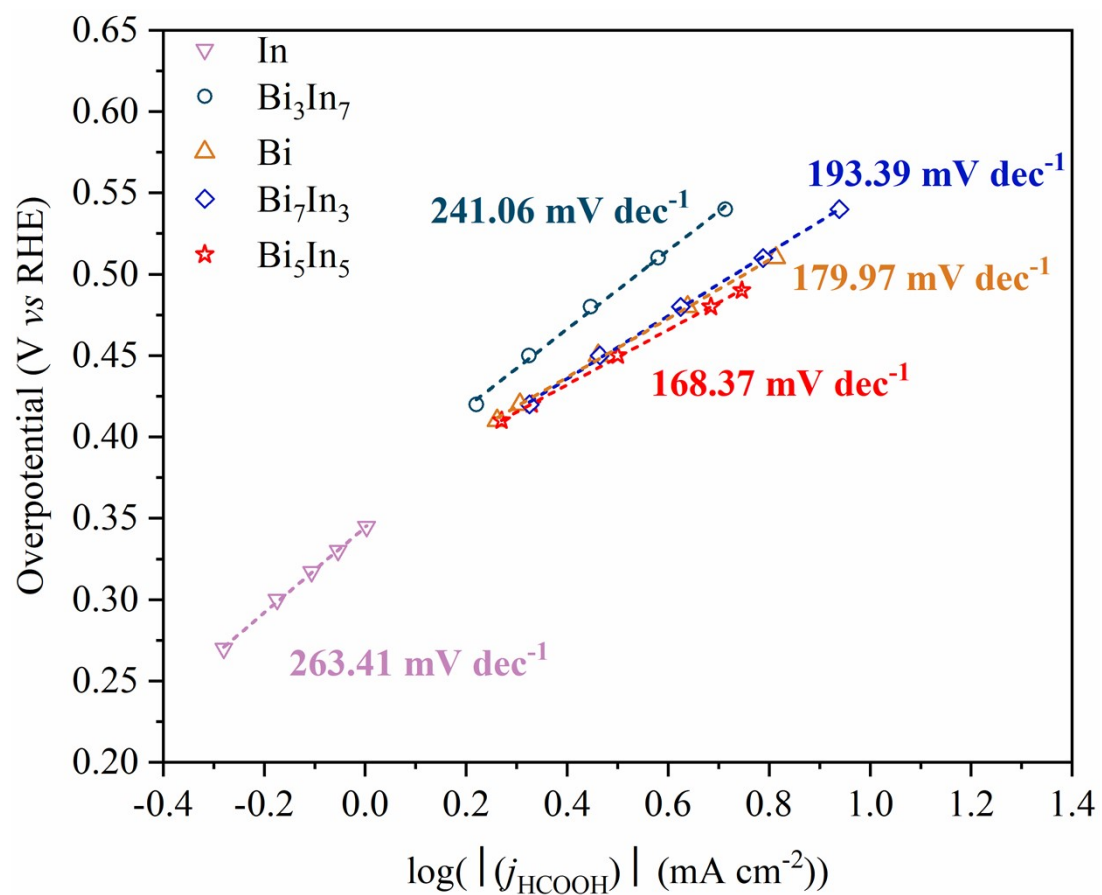


Fig. S25. Catalytic performance comparison with the recently reported catalysts.



**Fig. S26.** CV curves of the (a) Bi NFs, (b)  $\text{Bi}_7\text{In}_3$  NFs, (c)  $\text{Bi}_5\text{In}_5$  NPs, (d)  $\text{Bi}_3\text{In}_7$  NPs, and (e) In NFs.



**Fig. S27.** The Tafel slopes of different catalysts.

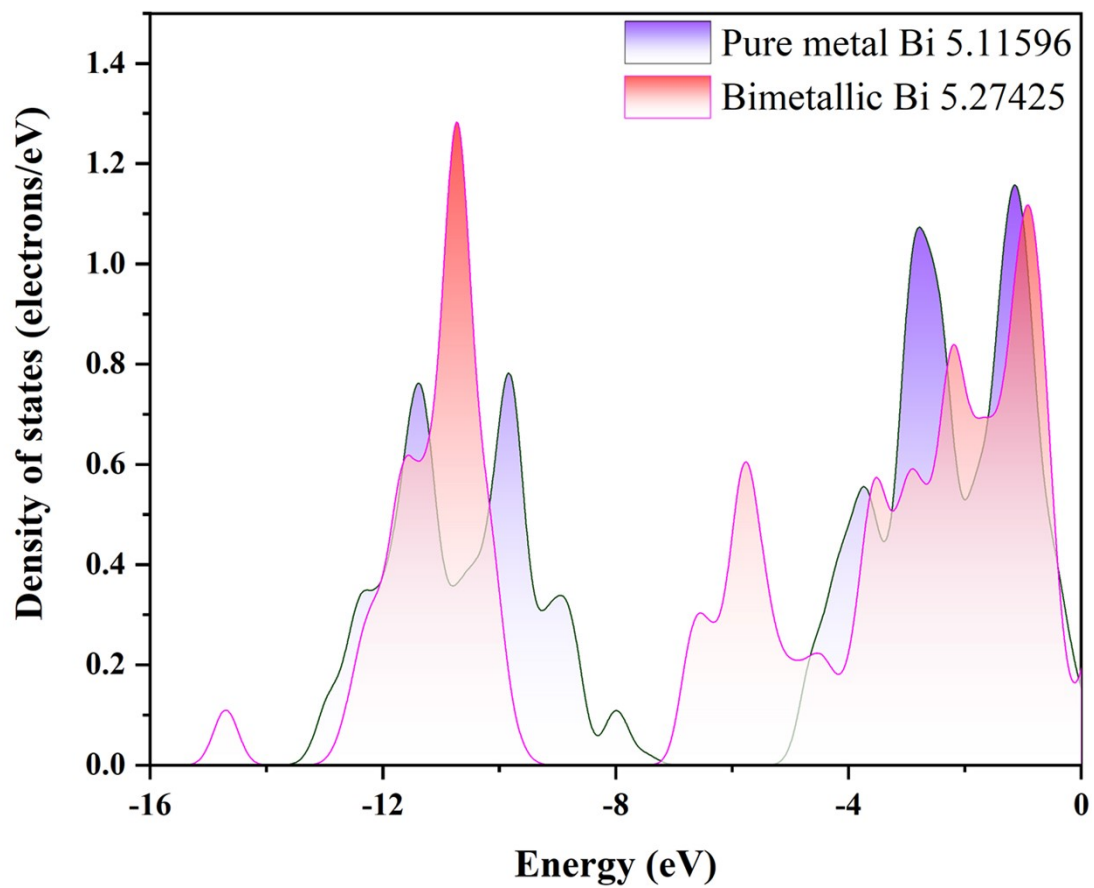
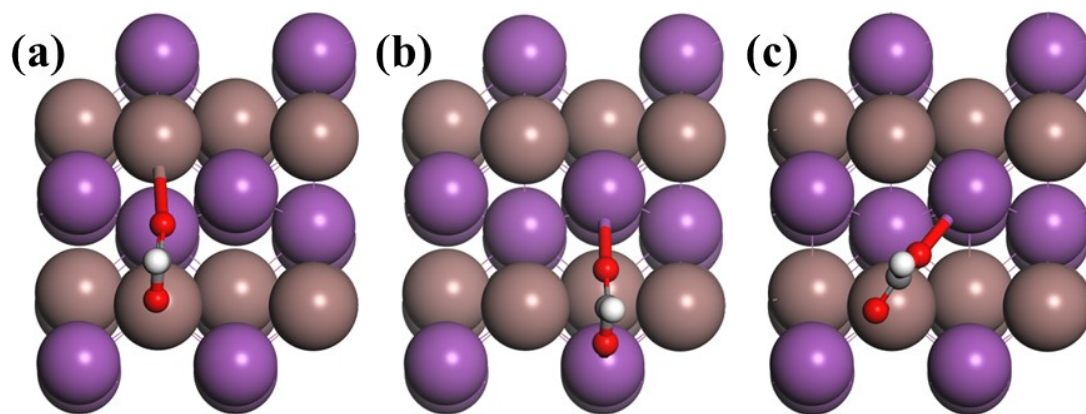
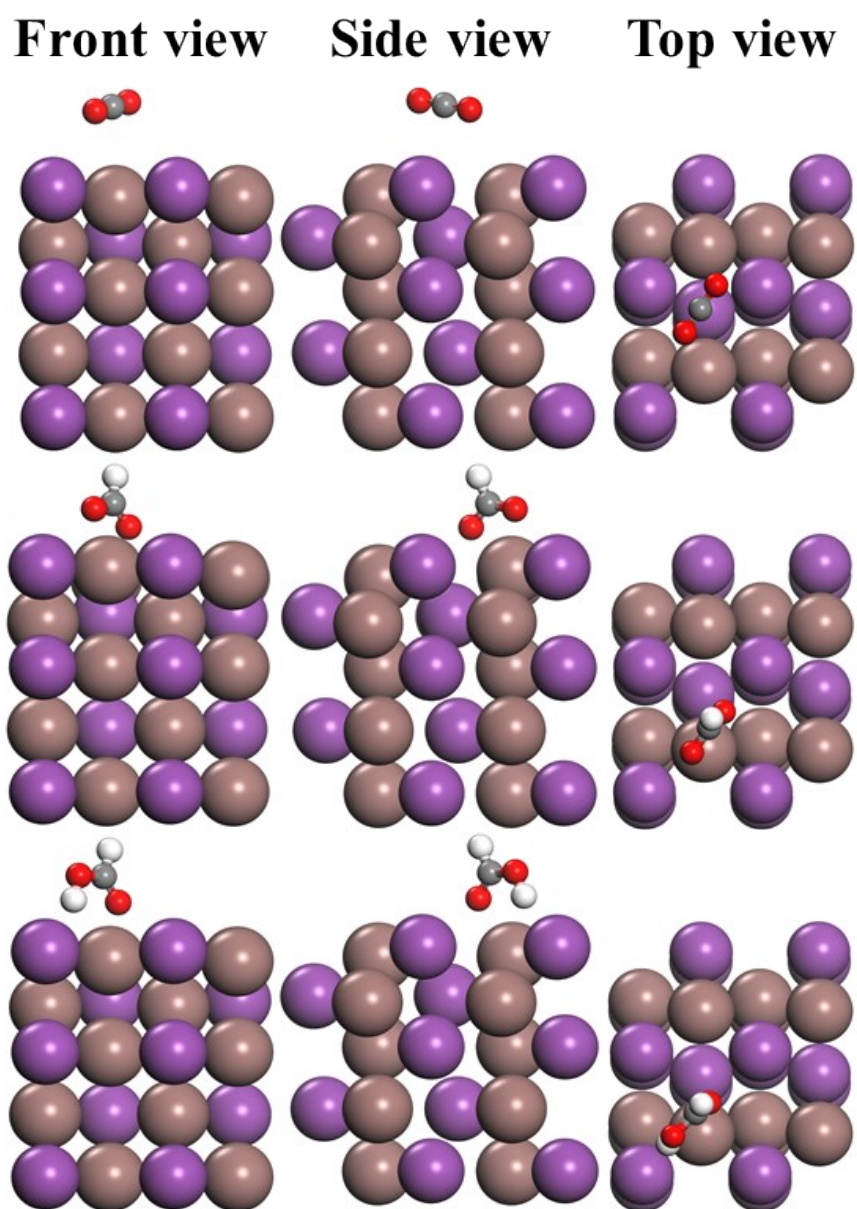


Fig. S28. Density of states for Bi atoms in InBi.



**Fig. S29.** \*OCHO intermediate adsorption sites of (a) In-In, (b) Bi-Bi, (c) In-Bi.



**Fig. S30.** Three-view Picture of DFT configurations for CO<sub>2</sub>\*, \*OCHO, and \*HCOOH on the InBi (200) surface.

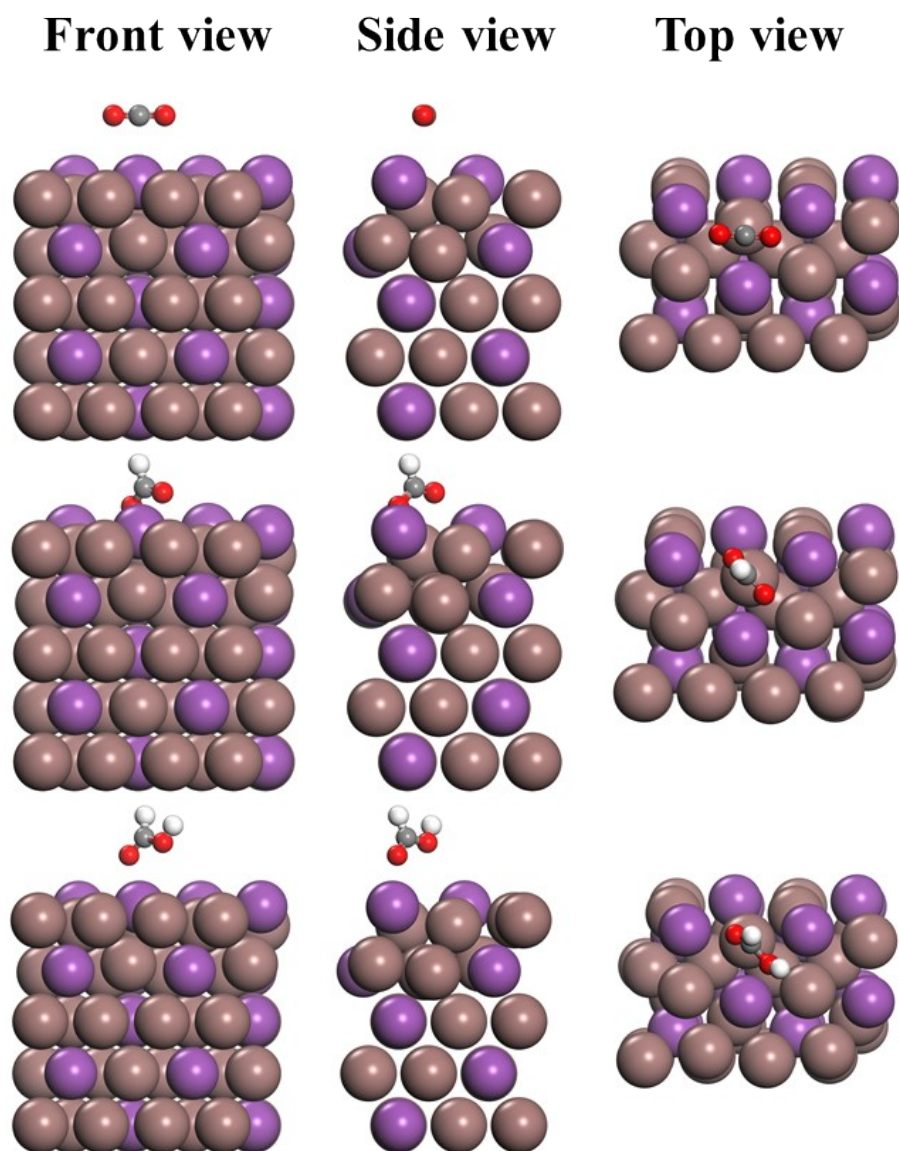


**Fig. S31.** Three-view Picture of DFT configurations for  $\text{CO}_2^*$ ,  $^*\text{OCHO}$ , and  $^*\text{HCOOH}$  on the  $\text{BiIn}_2$  (110) surface.

**Front view**      **Side view**      **Top view**

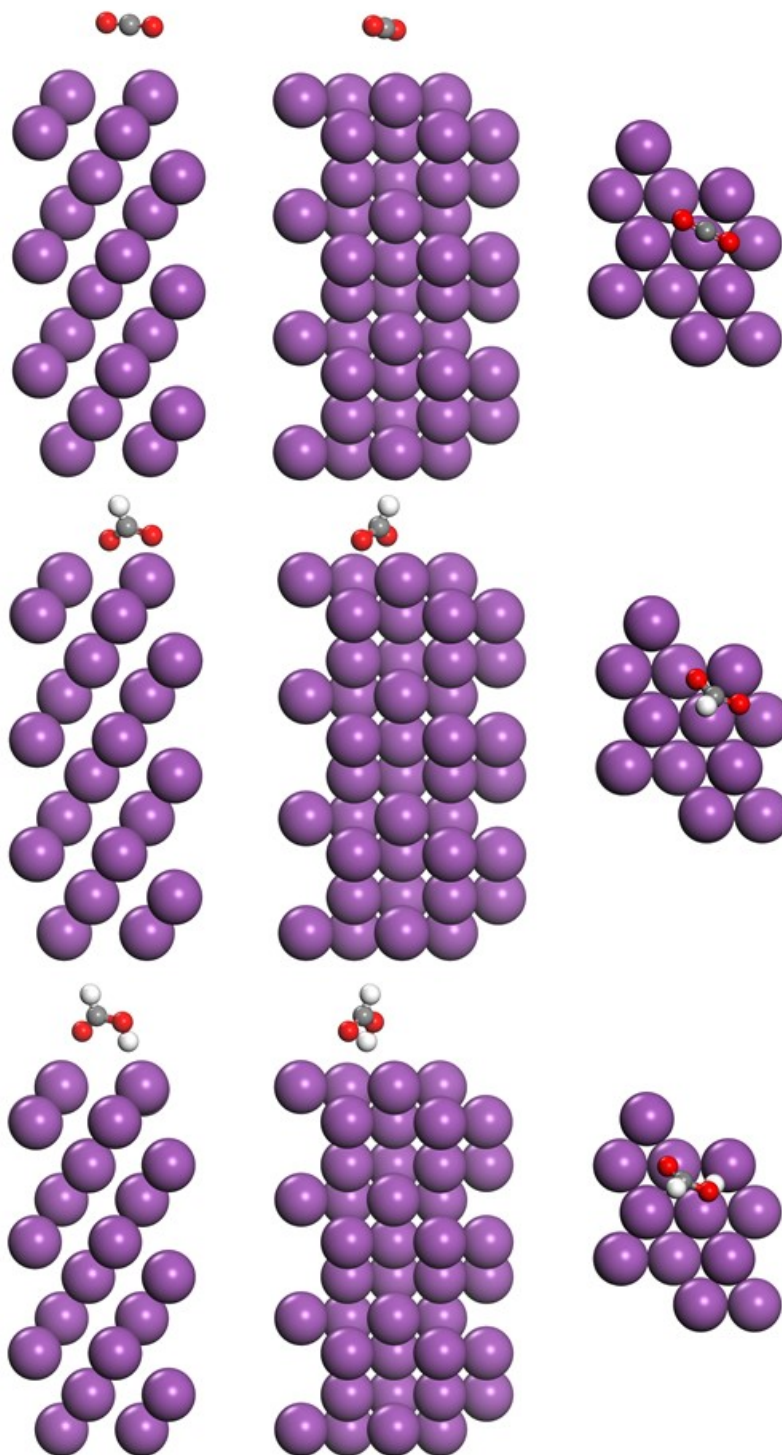


**Fig. S32.** Three-view Picture of DFT configurations for  $\text{CO}_2^*$ ,  $^*\text{OCHO}$ , and  $^*\text{HCOOH}$  on the Bi (003) surface.



**Front view**

**Side view**

**Top view**

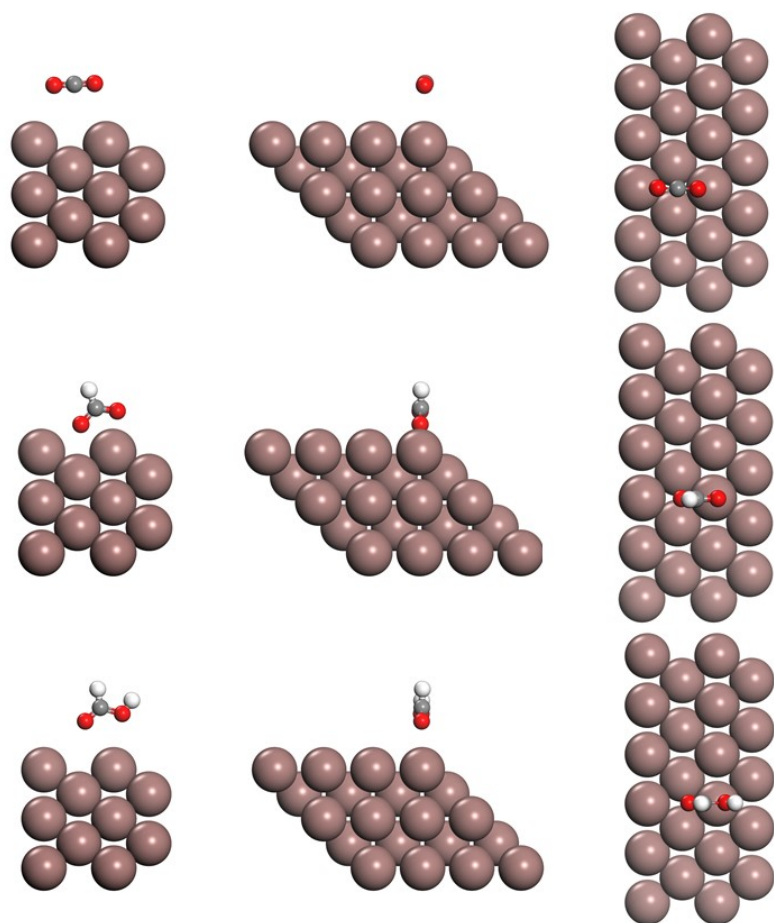


**Fig. S33.** Three-view Picture of DFT configurations for CO<sub>2</sub>\*, \*OCHO, and \*HCOOH on the In (112) surface.

**Table S1.** EDS elemental analysis of  $\text{In}_x\text{Bi}_y$  NFs.

Code	Atomic % (at%)	
	Bi	In
Bi	100	0
$\text{Bi}_7\text{In}_3$	67.38	32.62
$\text{Bi}_5\text{In}_5$	51.45	48.55
$\text{Bi}_3\text{In}_7$	31.56	68.44
In	100	0

**Table S2.** ICP analysis of  $\text{In}_x\text{Bi}_y$  NFs.

Code	Atomic % (at%)	
	Bi	In
$\text{Bi}_7\text{In}_3$	70.59	29.41
$\text{Bi}_5\text{In}_5$	50.98	49.02
$\text{Bi}_3\text{In}_7$	31.37	68.63

**Table S3.** The enthalpy of In-In, Bi-Bi, and In-Bi adsorption sites with \*OCHO intermediate.

	In-In	Bi-Bi	In-Bi
Final enthalpy (eV)	-44004.24994	-44004.22351	-44004.30767

**Table S4.** Calculated Gibbs free energy results of the intermediates on Bi, In, BiIn<sub>2</sub>, InBi

Free energy (eV)	*CO <sub>2</sub>	*OCHO	*HCOOH	HCOOH
Bi	-16899.39653	-16914.99642	-16931.08746	-1069.496642
In	-71253.59698	-71269.74023	-71285.39774	-1069.496642
BiIn <sub>2</sub>	-79179.30407	-79195.26181	-79211.07316	-1069.496642
InBi	-44060.45862	-44076.43317	-44092.26833	-1069.496642